BI-TP 2000/04
DESY 01-121
Edinburgh 2001/11
hep-ph/0109062

arXiv:hep-ph/0109062v2 14 Nov 2001

# Electroweak radiative corrections to W-boson production at hadron colliders

Stefan Dittmaier[†]

*Deutsches Elektronen-Synchrotron DESY,*
*D-22603 Hamburg, Germany*

Michael Krämer

*Department of Physics and Astronomy, University of Edinburgh,*
*Edinburgh EH9 3JZ, Scotland*

**Abstract:**

The complete set of electroweak $\mathcal{O}(\alpha)$ corrections to the Drell–Yan-like production of W bosons is calculated and compared to an approximation provided by the leading term of an expansion about the W-resonance pole. All relevant formulae are listed explicitly, and particular attention is paid to issues of gauge invariance and the instability of the W bosons. A detailed discussion of numerical results underlines the phenomenological importance of the electroweak corrections to W-boson production at the Tevatron and at the LHC. While the pole expansion yields a good description of resonance observables, it is not sufficient for the high-energy tail of transverse-momentum distributions, relevant for new-physics searches.

September 2001

---

[†]Heisenberg fellow of the Deutsche Forschungsgemeinschaft DFG.

# 1 Introduction

The Drell–Yan-like production of W bosons represents one of the cleanest processes with a large cross section at the Tevatron and at the LHC. This reaction is not only well suited for a precise determination of the W-boson mass $M_{\mathrm{W}}$, it also yields valuable information on the parton structure of the proton. Specifically, the accuracy of $\approx 15$–$20\,\mathrm{MeV}$ [1] in the $M_{\mathrm{W}}$ measurement envisaged at the LHC will improve upon the precision of $\approx 30\,\mathrm{MeV}$ to be achieved at LEP2 [2] and Tevatron Run II [3], and thus competes with the precision of the $M_{\mathrm{W}}$ measurement expected at a future $\mathrm{e^+e^-}$ collider [4]. Concerning quark distributions, precise measurements of rapidity distributions provide information over a wide range in $x$ [5]; a measurement of the d/u ratio would, in particular, be complementary to HERA results. The more direct determination of parton–parton luminosities instead of single parton distributions is even more precise [6]; extracting the corresponding luminosities from Drell–Yan-like processes allows one to predict related $q\bar{q}$ processes at the per-cent level.

Owing to the high experimental precision outlined above, the predictions for the processes $\mathrm{pp/p\bar{p}} \to \mathrm{W} \to l\nu_l$ should match per-cent accuracy; for specific observables the required theoretical accuracy is even higher. To this end, radiative corrections have to be included. In particular, it is important to treat final-state radiation carefully, since photon emission from the final-state lepton significantly changes the lepton momentum, which is used in the determination of the W-boson mass. A first step to include electroweak corrections was already made in Ref. [7], where effects of final-state radiation in the W-boson decay stage were taken into account. Those effects lead to a shift in the value of $M_{\mathrm{W}}$ of the order of $50$–$150\,\mathrm{MeV}$. The approximation of Ref. [7] was improved much later in Ref. [8], where the electroweak $\mathcal{O}(\alpha)$ corrections to resonant W-boson production [9] were discussed for W production at the Tevatron in detail. The $\mathcal{O}(\alpha)$ corrections are of the order of the known next-to-next-to-leading order (NNLO) QCD corrections [10] to Drell–Yan-like processes. In $\mathcal{O}(\alpha^2)$ only a study of two-photon radiation exists [11], while the virtual counterpart is completely unknown. Discussions of QCD corrections to Drell–Yan-like processes can be found in Refs. [12, 13] and references therein.

In this paper we present the complete calculation of the electroweak $\mathcal{O}(\alpha)$ corrections, including non-resonant contributions. In particular, we compare the full $\mathcal{O}(\alpha)$ correction to a *pole approximation* (similar to the one used in Refs. [8, 9]) that is based on the correction to the production of resonant W bosons. All relevant formulae are listed explicitly. Moreover, a discussion of numerical results is presented for the Tevatron (Run II) and for the LHC. Partial results of this analysis have already been presented in the LHC workshop report [14].

The paper is organized as follows. In Sect. 2 we set our conventions and provide analytical results for the parton-level subprocess. In particular, we describe the calculation of the complete and the "pole-approximated" $\mathcal{O}(\alpha)$ corrections. Different methods for treating the infrared and collinear singularities are presented and compared with each other. The hadronic cross section is discussed in Sect. 3. In Section 4 we present numerical results for W-boson production at the Tevatron and at the LHC. Our conclusions are given in Sect. 5. Finally, the appendices provide some supplementary formulae.

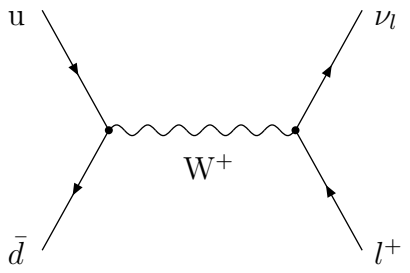


Figure 1: Lowest-order diagram for $u\bar{d} \to \mathrm{W}^+ \to \nu_l l^+$.

# 2 The parton process $u\bar{d} \to \mathrm{W}^+ \to \nu_l l^+(+\gamma)$

## 2.1 Conventions and lowest-order cross section

We consider the parton process

$$u(p_u, \tau_u) + \bar{d}(p_d, \tau_d) \;\to\; \nu_l(k_n, -) + l^+(k_l, \tau_l) \;\; [+\gamma(k, \lambda)], \tag{2.1}$$

where $u$ and $d$ generically denote the light up- and down-type quarks, $u = \mathrm{u}, \mathrm{c}$ and $d = \mathrm{d}, \mathrm{s}$. The lepton $l$ represents $l = \mathrm{e}, \mu, \tau$. The momenta and helicities of the corresponding particles are given in brackets. The Mandelstam variables are defined by

$$\hat{s} = (p_u + p_d)^2, \quad \hat{t} = (p_d - k_l)^2, \quad \hat{u} = (p_u - k_l)^2, \quad s_{\nu_l l} = (k_n + k_l)^2. \tag{2.2}$$

We neglect the fermion masses $m_u$, $m_d$, $m_l$ whenever possible, i.e. we keep these masses only as regulators in the logarithmic mass singularities originating from collinear photon emission or exchange. Obviously, we have $\hat{s} = s_{\nu_l l}$ for the non-radiative process $u\bar{d} \to \nu_l l^+$. In lowest order only the Feynman diagram shown in Fig. 1 contributes to the scattering amplitude, and the Born amplitude reads

$$\mathcal{M}_0 = \frac{e^2 V_{ud}^*}{2 s_\mathrm{w}^2} \, [\bar{v}_d \gamma^\mu \omega_- u_u] \, \frac{1}{\hat{s} - M_\mathrm{W}^2 + \mathrm{i} M_\mathrm{W} \Gamma_\mathrm{W}(\hat{s})} \, [\bar{u}_{\nu_l} \gamma_\mu \omega_- v_l] \,, \tag{2.3}$$

with an obvious notation for the Dirac spinors $\bar{v}_d$, etc., and the left-handed chirality projector $\omega_- = \frac{1}{2}(1 - \gamma_5)$. The electric unit charge is denoted by $e$, the weak mixing angle is fixed by the ratio $c_\mathrm{w}^2 = 1 - s_\mathrm{w}^2 = M_\mathrm{W}^2/M_\mathrm{Z}^2$ of the W- and Z-boson masses $M_\mathrm{W}$ and $M_\mathrm{Z}$, and $V_{ud}$ is the CKM matrix element for the $ud$ transition.

Strictly speaking, Eq. (2.3) already goes beyond lowest order, since the W-boson width $\Gamma_\mathrm{W}(\hat{s})$ results from the Dyson summation of all insertions of the (imaginary part of the) W self-energy. Defining the mass $M_\mathrm{W}$ and the width $\Gamma_\mathrm{W}$ of the W boson in the on-shell scheme (see e.g. Ref. [15]), the Dyson summation directly leads to a *running width*, i.e.

$$\Gamma_\mathrm{W}(\hat{s})|_\mathrm{run} = \Gamma_\mathrm{W} \frac{\hat{s}}{M_\mathrm{W}^2}. \tag{2.4}$$

On the other hand, a description of the resonance by an expansion about the complex pole in the complex $\hat{s}$ plane corresponds to a *constant width*, i.e.

$$\Gamma_\mathrm{W}(\hat{s})|_\mathrm{const} = \Gamma_\mathrm{W}. \tag{2.5}$$

In lowest order these two parametrizations of the resonance region are fully equivalent, but the corresponding values of the line-shape parameters $M_{\mathrm{W}}$ and $\Gamma_{\mathrm{W}}$ differ in higher orders [9, 16, 17],

$$M_{\mathrm{W}}^2|_{\mathrm{const}} = \left(M_{\mathrm{W}}^2 - \Gamma_{\mathrm{W}}^2 + \ldots\right)\Big|_{\mathrm{run}}, \qquad \Gamma_{\mathrm{W}}|_{\mathrm{const}} = \Gamma_{\mathrm{W}}\left(1 - \frac{\Gamma_{\mathrm{W}}^2}{2M_{\mathrm{W}}^2} + \ldots\right)\Big|_{\mathrm{run}}. \tag{2.6}$$

Since $M_{\mathrm{W}}|_{\mathrm{run}} - M_{\mathrm{W}}|_{\mathrm{const}} \approx 26\,\mathrm{MeV}$, it is necessary to state explicitly which parametrization is used in a precision determination of the W-boson mass from the W line-shape.

The differential lowest-order cross section is easily obtained by squaring the lowest-order matrix element $\mathcal{M}_0$ of (2.3),

$$\left(\frac{\mathrm{d}\hat{\sigma}_0}{\mathrm{d}\hat{\Omega}}\right) = \frac{1}{12}\,\frac{1}{64\pi^2\hat{s}}\,|\mathcal{M}_0|^2 = \frac{\alpha^2|V_{ud}|^2}{48 s_{\mathrm{W}}^4\,\hat{s}}\,\frac{\hat{u}^2}{|\hat{s} - M_{\mathrm{W}}^2 + \mathrm{i}M_{\mathrm{W}}\Gamma_{\mathrm{W}}(\hat{s})|^2}, \tag{2.7}$$

where the explicit factor 1/12 results from the average over the quark spins and colours, and $\hat{\Omega}$ is the solid angle of the outgoing $l^+$ in the parton centre-of-mass (CM) frame. The electromagnetic coupling $\alpha = e^2/(4\pi)$ can be set to different values according to different input-parameter schemes. It can be directly identified with the fine-structure constant $\alpha(0)$ or the running electromagnetic coupling $\alpha(Q^2)$ at a high-energy scale $Q$. For instance, it is possible to make use of the value of $\alpha(M_{\mathrm{Z}}^2)$ that is obtained by analyzing [18] the experimental ratio $R = \sigma(\mathrm{e}^+\mathrm{e}^- \to \mathrm{hadrons})/(\mathrm{e}^+\mathrm{e}^- \to \mu^+\mu^-)$. These choices are called $\alpha(0)$-*scheme* and $\alpha(M_{\mathrm{Z}}^2)$-*scheme*, respectively, in the following. Another value for $\alpha$ can be deduced from the Fermi constant $G_\mu$, yielding $\alpha_{G_\mu} = \sqrt{2}G_\mu M_{\mathrm{W}}^2 s_{\mathrm{W}}^2/\pi$; this choice is referred to as $G_\mu$-*scheme*. The differences between these schemes will become apparent in the discussion of the corresponding $\mathcal{O}(\alpha)$ corrections.

## 2.2 Virtual corrections

The virtual one-loop corrections comprise contributions of the transverse part of the $W$ self-energy $\Sigma_{\mathrm{T}}^W$, corrections to the two $Wdu$ and $W\nu_l l$ vertices, box diagrams, and counterterms. The explicit expression for $\Sigma_{\mathrm{T}}^W$ (in the 't Hooft–Feynman gauge) can, e.g., be found in Ref. [15]. The diagrams for the vertex and box corrections, which are shown in Fig. 2, were calculated using standard methods. The Feynman diagrams and amplitudes were generated with *FeynArts* [19]. The subsequent algebraic reduction [20] of the one-loop tensor integrals to scalar integrals was performed with *FeynCalc* [21], and the scalar integrals were evaluated using the methods and results of Ref. [22]. The algebraic part was checked numerically by a completely independent calculation, in which the amplitudes are expressed in terms of tensor coefficients using *Mathematica*, and the tensor reduction is done numerically. UV divergences are treated in dimensional regularization, and the IR singularity is regularized by an infinitesimal photon mass $m_\gamma$. The actual calculation is performed in 't Hooft–Feynman gauge using the on-shell renormalization scheme described in Ref. [15], where, in particular, all renormalization constants used in this paper can be found. As an additional check we have repeated the calculation within the background-field formalism [23] and found perfect agreement. In the following we sketch the structure of the virtual corrections and emphasize those points that are relevant for the treatment

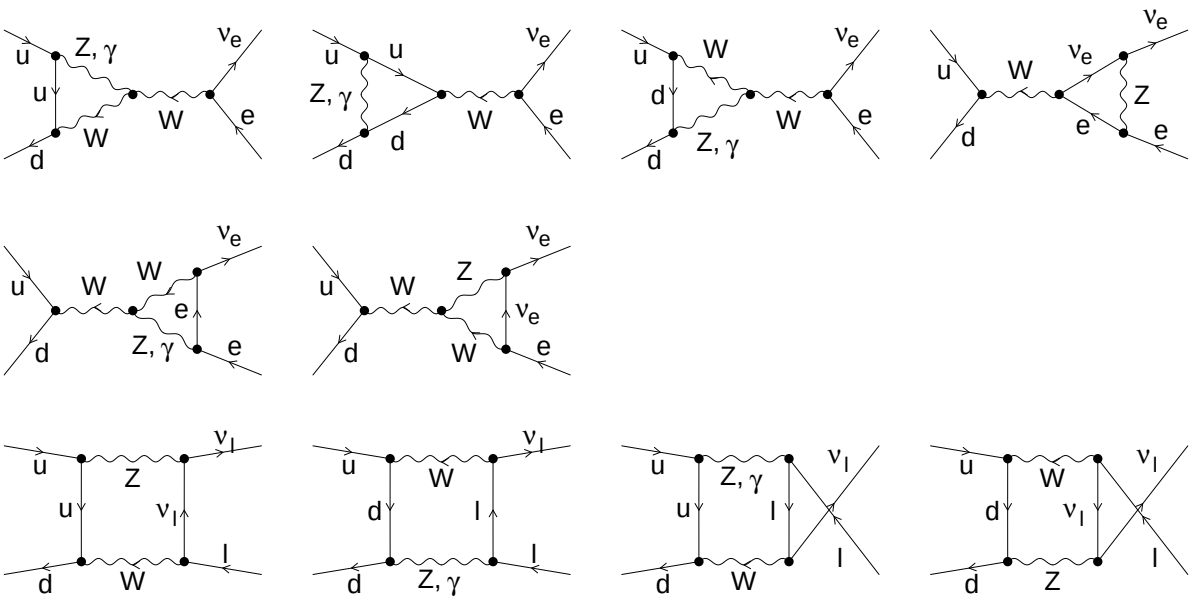


Figure 2: Diagrams for vertex and box corrections.

of the resonance and for the change from one input-parameter scheme to another. The complete expressions for the vertex and box corrections are provided in App. A.

While the self-energy and vertex corrections are proportional to the Dirac structure appearing in the lowest-order matrix element $\mathcal{M}_0$, the calculation of the box diagrams leads to additional combinations of Dirac chains. However, since the box diagrams are UV-finite, the four-dimensionality of space-time can be used to reduce all Dirac structures to the one of $\mathcal{M}_0$, see App. A.2. In summary, the complete one-loop amplitude $\mathcal{M}_1$ can be expressed in terms of a correction factor $\delta^{\text{virt}}$ times the lowest-order matrix element,

$$\mathcal{M}_1 = \delta^{\text{virt}} \mathcal{M}_0. \tag{2.8}$$

Thus, in $\mathcal{O}(\alpha)$ the squared matrix element reads

$$|\mathcal{M}_0 + \mathcal{M}_1|^2 = (1 + 2\,\text{Re}\{\delta^{\text{virt}}\})|\mathcal{M}_0|^2 + \ldots, \tag{2.9}$$

so that the Breit–Wigner factors are completely contained in the lowest-order factor $|\mathcal{M}_0|^2$. Note that the Dyson-summed imaginary part of the W self-energy, which appears as $\Gamma_{\text{W}}(\hat{s})$ in $\mathcal{M}_0$, is not double-counted, since only the real part of $\Sigma_{\text{T}}^{W}$ enters $\text{Re}\{\delta^{\text{virt}}\}$ in $\mathcal{O}(\alpha)$.[1] The correction factor $\delta^{\text{virt}}$ is decomposed into four different parts,

$$\delta^{\text{virt}} = \delta_{WW}(\hat{s}) + \delta_{Wdu}(\hat{s}) + \delta_{W\nu_l l}(\hat{s}) + \delta_{\text{box}}(\hat{s}, \hat{t}), \tag{2.10}$$

[1]Note also that only the imaginary parts induced by the fermion loops, which lead to the physical decay width in the resonance propagator, are resummed, while all other parts of $\Sigma_{\text{T}}^{W}$ are treated in $\mathcal{O}(\alpha)$. In this way the differences between the on-shell renormalization of the W-boson mass (see e.g. Ref. [15]) and other variants based on the complex pole position in the inverse W propagator are of $\mathcal{O}(\alpha^2)$, and thus beyond the accuracy of our calculation. In particular, the problems [24] with the resummation of loops containing photon exchange are avoided.

according to the splitting into self-energy, vertex, and box diagrams.

The $W$ self-energy correction reads

$$\delta_{WW}(\hat{s}) = -\frac{\Sigma_{\mathrm{T}}^{W}(\hat{s}) - \delta M_{\mathrm{W}}^2}{\hat{s} - M_{\mathrm{W}}^2} - \delta Z_W, \tag{2.11}$$

where the explicit expression for the unrenormalized self-energy $\Sigma_{\mathrm{T}}^{W}$ is given in Eq. (B.4) of Ref. [15]. In the on-shell renormalization scheme the renormalization constants for the W-boson mass and field, $\delta M_{\mathrm{W}}^2$ and $\delta Z_W$, are directly related to $\Sigma_{\mathrm{T}}^{W}$.

The vertex corrections are given by

$$\delta_{Wdu}(\hat{s}) = F_{Wdu}(\hat{s}) + \delta_{Wdu}^{\mathrm{ct}}, \qquad \delta_{W\nu_l l}(\hat{s}) = F_{W\nu_l l}(\hat{s}) + \delta_{W\nu_l l}^{\mathrm{ct}}, \tag{2.12}$$

where the explicit expression for the form factor $F_{Wff'}(\hat{s})$ is given in App. A.1. The counterterm $\delta_{Wff'}^{\mathrm{ct}}$ for the $Wff'$ vertex depends on the input-parameter scheme. In the $\alpha(0)$-scheme (i.e. the usual on-shell scheme), it is given by[2]

$$\delta_{Wff'}^{\mathrm{ct}}|_{\alpha(0)} = \delta Z_e - \frac{\delta s_{\mathrm{W}}}{s_{\mathrm{W}}} + \frac{1}{2}(\delta Z_W + \delta Z^{f,\mathrm{L}} + \delta Z^{f',\mathrm{L}}). \tag{2.13}$$

The wave-function renormalization constants $\delta Z^{f,\mathrm{L}}$ and $\delta Z^{f',\mathrm{L}}$ are obtained from the (left-handed part of) the fermion self-energies, and the renormalization of the weak mixing angle, i.e. $\delta s_{\mathrm{W}}$, is connected to the mass renormalization of the gauge-boson masses. The charge renormalization constant $\delta Z_e$ contains logarithms of the light-fermion masses, inducing large corrections proportional to $\alpha \ln(m_f^2/\hat{s})$, which are related to the running of the electromagnetic coupling $\alpha(Q^2)$ from $Q = 0$ to a high-energy scale. In order to render these quark-mass logarithms meaningful, it is necessary to adjust these masses to the asymptotic tail of the hadronic contribution to the vacuum polarization $\Pi^{AA}$ of the photon. Using $\alpha(M_{\mathrm{Z}}^2)$, as defined in Ref. [18], as input this adjustment is implicitly incorporated, and the counterterm reads

$$\delta_{Wff'}^{\mathrm{ct}}|_{\alpha(M_{\mathrm{Z}}^2)} = \delta_{Wff'}^{\mathrm{ct}}|_{\alpha(0)} - \frac{1}{2}\Delta\alpha(M_{\mathrm{Z}}^2), \tag{2.14}$$

where

$$\Delta\alpha(Q^2) = \Pi_{f\neq\mathrm{t}}^{AA}(0) - \mathrm{Re}\{\Pi_{f\neq\mathrm{t}}^{AA}(Q^2)\}, \tag{2.15}$$

with $\Pi_{f\neq\mathrm{t}}^{AA}$ denoting the photonic vacuum polarization induced by all fermions other than the top quark (see also Ref. [15]). In contrast to the $\alpha(0)$-scheme the counterterm $\delta_{Wff'}^{\mathrm{ct}}|_{\alpha(M_{\mathrm{Z}}^2)}$ does not involve light quark masses, since all corrections of the form $\alpha^n \ln^n(m_f^2/\hat{s})$ are absorbed in the lowest-order cross section parametrized by $\alpha(M_{\mathrm{Z}}^2) = \alpha(0)/[1 - \Delta\alpha(M_{\mathrm{Z}}^2)]$. In the $G_\mu$-scheme, the transition from $\alpha(0)$ to $G_\mu$ is ruled by the quantity $\Delta r$ [15, 25], which is deduced from muon decay,

$$\alpha_{G_\mu} = \frac{\sqrt{2} G_\mu M_{\mathrm{W}}^2 s_{\mathrm{W}}^2}{\pi} = \alpha(0)(1 + \Delta r) \; + \; \mathcal{O}(\alpha^3). \tag{2.16}$$

[2]We consistently set the CKM matrix to the unit matrix in the correction factor $\delta^{\mathrm{virt}}$, since mixing effects in the $\mathcal{O}(\alpha)$ corrections are negligible. This means that the CKM matrix appears only in the global factor $|V_{ud}|^2$ to the $\mathcal{O}(\alpha)$-corrected parton cross section.

Therefore, the counterterm $\delta^{\rm ct}_{Wff'}$ reads

$$\delta^{\rm ct}_{Wff'}|_{G_\mu} = \delta^{\rm ct}_{Wff'}|_{\alpha(0)} - \frac{1}{2}\Delta r. \tag{2.17}$$

Since $\Delta\alpha(M_{\rm Z}^2)$ is explicitly contained in $\Delta r$, the large fermion-mass logarithms are also resummed in the $G_\mu$-scheme. Moreover, the lowest-order cross section in $G_\mu$-parametrization absorbs large universal corrections induced by the $\rho$-parameter.

The box correction $\delta_{\rm box}(\hat{s},\hat{t})$ is the only virtual correction that depends also on the scattering angle, i.e. on the variables $\hat{t}$ and $\hat{u} = -\hat{s} - \hat{t}$. The explicit expression for $\delta_{\rm box}(\hat{s},\hat{t})$ is given in App. A.2.

Despite the separation of the resonance pole $(\hat{s} - M_{\rm W}^2)^{-1}$ from the correction factor $\delta^{\rm virt}$ in (2.8), $\delta^{\rm virt}$ still contains logarithms $\ln(\hat{s} - M_{\rm W}^2 + {\rm i}\epsilon)$ that are singular on resonance. Since these singularities would be cured by a Dyson summation of the $W$ self-energy inside the loop diagrams, we substitute

$$\ln(\hat{s} - M_{\rm W}^2 + {\rm i}\epsilon) \;\to\; \ln(\hat{s} - M_{\rm W}^2 + {\rm i}M_{\rm W}\Gamma_{\rm W}) \tag{2.18}$$

with a fixed width everywhere, independent of the use of a fixed or running width in lowest order. In principle, also a running width could be used on the r.h.s., but the difference to the fixed width is of two-loop order, and thus beyond the accuracy of our calculation. The substitution (2.18) does not disturb the gauge-invariance properties of the one-loop amplitude $\mathcal{M}_1$, i.e. its gauge-parameter independence and the validity of SU(2)×U(1) Ward identities. The reason is that the sum of all terms in $\mathcal{M}_1$ proportional to $\ln(\hat{s} - M_{\rm W}^2 + {\rm i}\epsilon)$ separately fulfills the (algebraic) relations arising from gauge invariance, since this logarithm is the only resonant (and thus a unique) term in the relative correction $\delta^{\rm virt}$.

## 2.3 Virtual correction in pole approximation

If one is only interested in the production of (nearly) resonant W bosons, the electroweak corrections can be approximated by an expansion [26] about the resonance pole, which is located in the complex $\hat{s}$ plane at $M_{\rm W}^2 - {\rm i}M_{\rm W}\Gamma_{\rm W}$ up to higher-order terms. The approximation of taking into account only the leading term of this expansion is called *pole approximation* (PA) and should not be confused with the on-shell approximation for the W bosons. In contrast to the PA, the on-shell approximation, where the W bosons are assumed to be stable, does not provide a description of the W line-shape. In the following we construct a PA for the virtual correction factor $\delta^{\rm virt}$ in the same way as a *double-pole approximation* was constructed in Ref. [27] for the more complicated case of W-pair production in $\mathrm{e^+e^-}$ annihilation, $\mathrm{e^+e^-} \to \mathrm{WW} \to 4\,\mathrm{fermions}$. In this formulation the PA is only applied to the virtual corrections, while the real corrections are based on the full photon-emission matrix element, as described in the next section. In principle, it is also possible to construct a PA for the real corrections, as for instance described in Ref. [28] for $\mathrm{ee} \to \mathrm{WW}$.[3] However, we prefer to make use of the full matrix elements, as it was also done in the variant of the PA used in Ref. [8] for W production in hadronic collisions.

[3] More details about the pole expansions that are used in practice are reviewed in Ref. [29].

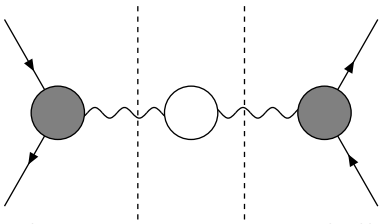


Figure 3: Generic diagram for factorizable corrections.

In the PA the virtual corrections to $u\bar{d} \to \mathrm{W} \to \nu_l l^+$ can be classified into two categories. The first category comprises the corrections to the production and the decay of an on-shell W boson. Owing to the independence of these subprocesses, these corrections are called *factorizable*. All contributing Feynman graphs are of the generic form shown in Fig. 3. By definition, the factorizable corrections receive only contributions from the $W$ self-energy and the $Wff'$ vertex corrections. The corresponding correction factor $\delta_{\mathrm{fact}}^{\mathrm{virt}}$ is obtained from $\delta_{WW}(\hat{s})$ and $\delta_{Wff'}(\hat{s})$ by setting $\hat{s} = M_{\mathrm{W}}^2$ and $\Gamma_{\mathrm{W}} = 0$. Since we have $\delta_{WW}(M_{\mathrm{W}}^2)|_{\Gamma_{\mathrm{W}}=0} = 0$ in the complete on-shell renormalization scheme, we get

$$\delta_{\mathrm{fact}}^{\mathrm{virt}} = \delta_{Wdu}(M_{\mathrm{W}}^2)|_{\Gamma_{\mathrm{W}}=0} + \delta_{W\nu_l l}(M_{\mathrm{W}}^2)|_{\Gamma_{\mathrm{W}}=0}. \tag{2.19}$$

Since the vertex corrections for on-shell W bosons correspond to physical S-matrix elements, both contributions to the factorizable corrections are gauge-invariant. Note that $\delta_{\mathrm{fact}}^{\mathrm{virt}}$ is a constant factor, neither depending on the scattering energy nor on the scattering angle. Moreover, $\delta_{\mathrm{fact}}^{\mathrm{virt}}$ contains IR singularities originating from the logarithms of (2.18); these terms are connected to photon emission from on-shell W bosons and are regularized by the infinitesimal photon mass $m_\gamma$.

The second category of corrections in the PA are called *non-factorizable* [30, 31] and comprise all remaining resonant contributions, i.e. all terms in $\delta^{\mathrm{virt}}$ that are non-vanishing for $\hat{s} \to M_{\mathrm{W}}^2$ and $\Gamma_{\mathrm{W}} \to 0$,

$$\delta_{\mathrm{nonfact}}^{\mathrm{virt}}(\hat{s},\hat{t}) = \delta^{\mathrm{virt}}|_{\hat{s}\to M_{\mathrm{W}}^2,\Gamma_{\mathrm{W}}\to 0} - \delta_{\mathrm{fact}}^{\mathrm{virt}}. \tag{2.20}$$

Here $\delta^{\mathrm{virt}}|_{\hat{s}\to M_{\mathrm{W}}^2,\Gamma_{\mathrm{W}}\to 0}$ results from the full off-shell correction $\delta^{\mathrm{virt}}$ upon taking the asymptotic limits $(\hat{s} - M_{\mathrm{W}}^2) \to 0$ and $\Gamma_{\mathrm{W}} \to 0$ while keeping the ratio $(\hat{s} - M_{\mathrm{W}}^2)/(M_{\mathrm{W}}\Gamma_{\mathrm{W}})$ fixed. As can be shown by simple power counting [31], only loop diagrams with an internal photon contribute. The relevant diagrams for $u\bar{d} \to \mathrm{W} \to \nu_l l^+$ are shown in Fig. 4. Since also box diagrams are involved, production and decay do not proceed independently, and the terminology *non-factorizable* is justified. The limit $\hat{s} \to M_{\mathrm{W}}^2$ for the pole expansion has to be defined carefully, because $\hat{s}$ is not the only kinematical variable. The variables $\hat{t}$ and $\hat{u}$, which are related to the scattering angle $\hat{\theta}$ of the parton CM frame, range within $-\hat{s} < \hat{t}, \hat{u} < 0$ and are related to $\hat{s}$ by $\hat{s} + \hat{t} + \hat{u} = 0$. Therefore, changing $\hat{s}$ while keeping $\hat{t}$ and $\hat{u}$ fixed is inconsistent in general. We circumvent this problem by taking $\hat{s} \to M_{\mathrm{W}}^2$ for fixed scattering angle $\hat{\theta}$, resulting in the replacements

$$\hat{t} \to \hat{t}_{\mathrm{res}} = \hat{t}\,\frac{M_{\mathrm{W}}^2}{\hat{s}} = -M_{\mathrm{W}}^2 \sin^2\tfrac{\hat{\theta}}{2}, \qquad \hat{u} \to \hat{u}_{\mathrm{res}} = \hat{u}\,\frac{M_{\mathrm{W}}^2}{\hat{s}} = -M_{\mathrm{W}}^2 \cos^2\tfrac{\hat{\theta}}{2}. \tag{2.21}$$

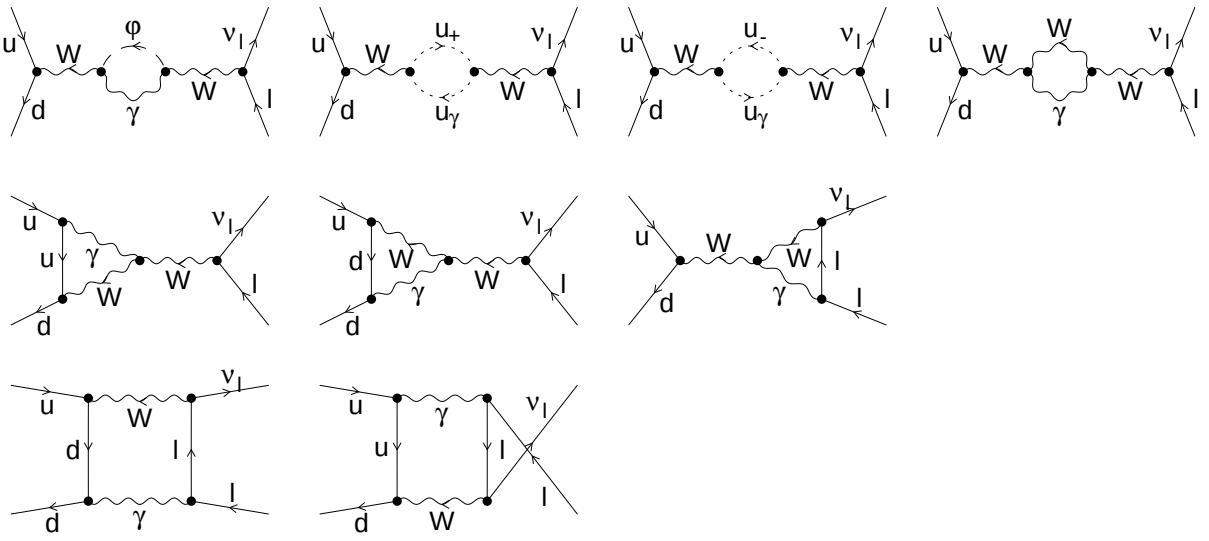


Figure 4: Diagrams for non-factorizable corrections ($\varphi$ is the would-be Goldstone partner to the W boson, and $\mathrm{u}_\pm$, $\mathrm{u}_\gamma$ denote Faddeev–Popov ghosts).

The actual calculation of $\delta^{\mathrm{virt}}_{\mathrm{nonfact}}$ is performed as described in Ref. [31] in detail. The final result is

$$\begin{aligned}\delta^{\mathrm{virt}}_{\mathrm{nonfact}}(\hat{s},\hat{t}) = -\frac{\alpha}{2\pi}\Bigg\{&-2 + Q_d\,\mathrm{Li}_2\Big(1+\frac{M_\mathrm{W}^2}{\hat{t}_{\mathrm{res}}}\Big) - Q_u\,\mathrm{Li}_2\Big(1+\frac{M_\mathrm{W}^2}{\hat{u}_{\mathrm{res}}}\Big)\\ &+ 2\ln\Big(\frac{M_\mathrm{W}^2 - \mathrm{i}M_\mathrm{W}\Gamma_\mathrm{W} - \hat{s}}{m_\gamma M_\mathrm{W}}\Big)\Big[1 + Q_d\ln\Big(-\frac{M_\mathrm{W}^2}{\hat{t}_{\mathrm{res}}}\Big) - Q_u\ln\Big(-\frac{M_\mathrm{W}^2}{\hat{u}_{\mathrm{res}}}\Big)\Big]\Bigg\},\end{aligned} \tag{2.22}$$

where

$$\mathrm{Li}_2(x) = -\int_0^x \frac{\mathrm{d}t}{t}\ln(1-t), \qquad |\arg(1-x)| < \pi, \tag{2.23}$$

is the usual dilogarithm, and $Q_f$ denotes the electric charge of the fermion $f$. In (2.22) we made use of $Q_l = Q_d - Q_u$. We note that $\delta^{\mathrm{virt}}_{\mathrm{nonfact}}$ is, by definition, a gauge-invariant quantity. It does not involve mass singularities of the fermions, but it is IR-singular. More precisely, the IR-singular term proportional to $\alpha\ln(m_\gamma)$ exactly compensates the artificially created IR singularity in $\delta^{\mathrm{virt}}_{\mathrm{fact}}$ by setting $\hat{s} = M_\mathrm{W}^2$ and $\Gamma_\mathrm{W} \to 0$ there, and these $\alpha\ln(m_\gamma)$ terms of $\delta^{\mathrm{virt}}_{\mathrm{fact}}$ are replaced by the correct logarithms $\alpha\ln(\hat{s} - M_\mathrm{W}^2 + \mathrm{i}M_\mathrm{W}\Gamma_\mathrm{W})$ after $\delta^{\mathrm{virt}}_{\mathrm{nonfact}}$ is added.

In summary, the PA for the virtual correction factor reads

$$\delta^{\mathrm{virt}}_{\mathrm{PA}} = \delta^{\mathrm{virt}}_{\mathrm{fact}} + \delta^{\mathrm{virt}}_{\mathrm{nonfact}}(\hat{s},\hat{t}) \tag{2.24}$$

with $\delta^{\mathrm{virt}}_{\mathrm{fact}}$ and $\delta^{\mathrm{virt}}_{\mathrm{nonfact}}$ given in (2.19) and (2.22), respectively. The uncertainty induced by omitting non-resonant corrections can be estimated naively by

$$\delta^{\mathrm{virt}}_{\mathrm{PA}} - \delta^{\mathrm{virt}} \sim \frac{\alpha}{\pi}\max\left\{\frac{\Gamma_\mathrm{W}}{M_\mathrm{W}}, \ln\Big(\frac{\hat{s}}{M_\mathrm{W}^2}\Big), \ln^2\Big(\frac{\hat{s}}{M_\mathrm{W}^2}\Big)\right\}, \tag{2.25}$$

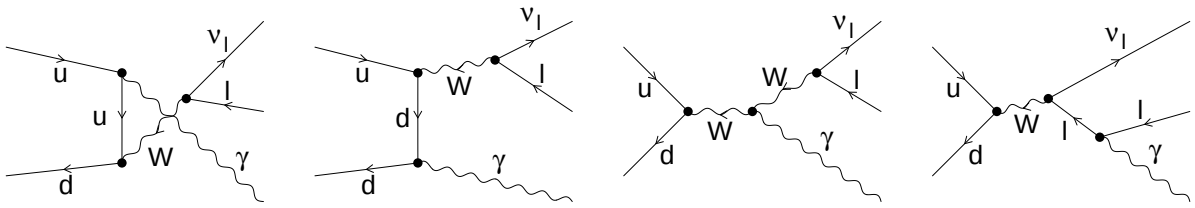


Figure 5: Diagrams for real-photon emission.

where the factor $\Gamma_{\mathrm{W}}/M_{\mathrm{W}}$ results from the neglect of non-resonant contributions near resonance and the logarithms account for typical enhancements away from resonance.

Finally, we note that we have analytically compared the PA for the virtual corrections worked out in this section with the results presented in Ref. [9]. Apart from non-resonant contributions, which go beyond the validity of the PA, both results agree.[4]

## 2.4 Real-photon emission

Real-photonic corrections are induced by the diagrams shown in Fig. 5. In the calculation of the corresponding amplitudes it is mandatory to respect the Ward identity for the external photon, i.e. electromagnetic current conservation. Writing the amplitudes as $\mathcal{M}_\gamma(\lambda) = \varepsilon^*_\mu(k,\lambda)T^\mu$ with $\varepsilon^*_\mu$ denoting the polarization vector of the outgoing photon, this Ward identity reads $k_\mu T^\mu = 0$. If the W width is zero, this identity is trivially fulfilled. This remains even true for a constant width, since the W-boson mass appears only in the W propagator denominators, i.e. the substitution $M^2_{\mathrm{W}} \to M^2_{\mathrm{W}} - \mathrm{i}M_{\mathrm{W}}\Gamma_{\mathrm{W}}$ is a consistent reparametrization of the amplitude in this case. However, if a running W width is introduced naively, i.e. in the W propagators only, the Ward identity is violated. The Ward identity can be restored by taking into account the part of the fermion-loop correction to the $\gamma WW$ vertex that corresponds to the fermion loops in the $W$ self-energy leading to the width in the propagator [17, 32]. In Ref. [33] it was shown that this modification simply amounts to the multiplication of the $\gamma WW$ vertex by the factor

$$f_{\gamma WW}|_{\mathrm{run}} = 1 + \mathrm{i}\frac{\Gamma_{\mathrm{W}}}{M_{\mathrm{W}}} \tag{2.26}$$

if the photon is on shell ($k^2 = 0$). By construction [17, 32, 33], the width $\Gamma_{\mathrm{W}}$ appearing in $f_{\gamma WW}|_{\mathrm{run}}$ as well as in the W propagator is the lowest-order width, since it results from the imaginary part of the W self-energy at one loop. Since, however, for the special case of an on-shell photon the relevant imaginary parts are completely parametrized by the ratio $\Gamma_{\mathrm{W}}/M_{\mathrm{W}}$, the Ward identity is fulfilled for any numerical value of $\Gamma_{\mathrm{W}}$. Therefore, we are allowed to use a value for $\Gamma_{\mathrm{W}}$ that includes also QCD and electroweak radiative corrections. For later convenience, we define

$$f_{\gamma WW}|_{\mathrm{const}} = 1. \tag{2.27}$$

In addition to the U(1) Ward identity for the external photon, an SU(2) Ward identity [17, 32] becomes relevant for effectively longitudinally polarized W bosons in W$\gamma$

[4]There is a misprint in Eq. (D.45) in Ref. [9]: the factor 2 in front of the $Q_{i'}Q_{f'}[(f,i) \to (f',i')]$, $Q_{i'}Q_f[(i,t) \to (i',u)]$ and $Q_iQ_{f'}[(f,t) \to (f',u)]$ terms needs to be removed.

production at high energies, where the lepton current $[\bar{u}_{\nu_l}\gamma_\mu\omega_- v_l]$ becomes proportional to the W momentum $k_{\mathrm{W}} = k_n + k_l$. As can be checked easily, this Ward identity is maintained in the above treatment of the W width as well.

The helicity amplitudes $\mathcal{M}_\gamma^{\tau_u\tau_d\tau_l}(\lambda)$ for the radiative process $u\bar{d} \to \nu_l l^+\gamma$ can be written in a very compact way using the Weyl-van der Waerden spinor formalism. Adopting the conventions of Ref. [34], we obtain

$$\begin{aligned}
\mathcal{M}_\gamma^{-+-}(+1) = {} & \frac{\sqrt{2}e^3 V_{ud}^*}{s_{\mathrm{W}}^2}\langle p_d k_n\rangle^2 \Big\{ -\frac{Q_u\langle k_n k_l\rangle^*}{[s_{\nu_l l} - M_{\mathrm{W}}^2 + \mathrm{i}M_{\mathrm{W}}\Gamma_{\mathrm{W}}(s_{\nu_l l})]\langle p_u k\rangle\langle p_d k\rangle} \\
& + \frac{1}{\hat{s} - M_{\mathrm{W}}^2 + \mathrm{i}M_{\mathrm{W}}\Gamma_{\mathrm{W}}(\hat{s})}\left[\frac{Q_l\langle p_u p_d\rangle^*}{\langle k k_n\rangle\langle k k_l\rangle} + \frac{(Q_d - Q_u)\langle p_u k_l\rangle^*}{\langle p_d k\rangle\langle k k_n\rangle}\right] \\
& + \frac{f_{\gamma\mathrm{WW}}(Q_u - Q_d)\langle k_n k_l\rangle^*\langle p_u k\rangle^*}{[\hat{s} - M_{\mathrm{W}}^2 + \mathrm{i}M_{\mathrm{W}}\Gamma_{\mathrm{W}}(\hat{s})][s_{\nu_l l} - M_{\mathrm{W}}^2 + \mathrm{i}M_{\mathrm{W}}\Gamma_{\mathrm{W}}(s_{\nu_l l})]\langle p_d k\rangle}\Big\}, \\
\mathcal{M}_\gamma^{-+-}(-1) = {} & \frac{\sqrt{2}e^3 V_{ud}^*}{s_{\mathrm{W}}^2}(\langle p_u k_l\rangle^*)^2 \Big\{ -\frac{Q_d\langle k_n k_l\rangle}{[s_{\nu_l l} - M_{\mathrm{W}}^2 + \mathrm{i}M_{\mathrm{W}}\Gamma_{\mathrm{W}}(s_{\nu_l l})]\langle p_u k\rangle^*\langle p_d k\rangle^*} \\
& + \frac{1}{\hat{s} - M_{\mathrm{W}}^2 + \mathrm{i}M_{\mathrm{W}}\Gamma_{\mathrm{W}}(\hat{s})}\left[\frac{Q_{\nu_l}\langle p_u p_d\rangle}{\langle k k_n\rangle^*\langle k k_l\rangle^*} + \frac{(Q_d - Q_u)\langle p_d k_n\rangle}{\langle p_u k\rangle^*\langle k k_l\rangle^*}\right] \\
& + \frac{f_{\gamma\mathrm{WW}}(Q_d - Q_u)\langle k_n k_l\rangle\langle p_d k\rangle}{[\hat{s} - M_{\mathrm{W}}^2 + \mathrm{i}M_{\mathrm{W}}\Gamma_{\mathrm{W}}(\hat{s})][s_{\nu_l l} - M_{\mathrm{W}}^2 + \mathrm{i}M_{\mathrm{W}}\Gamma_{\mathrm{W}}(s_{\nu_l l})]\langle p_u k\rangle^*}\Big\}. \qquad (2.28)
\end{aligned}$$

The amplitudes for the other helicity channels vanish for massless fermions. The spinor products are defined by

$$\langle pq\rangle = \epsilon^{AB} p_A q_B = 2\sqrt{p_0 q_0}\left[\mathrm{e}^{-\mathrm{i}\phi_p}\cos\frac{\theta_p}{2}\sin\frac{\theta_q}{2} - \mathrm{e}^{-\mathrm{i}\phi_q}\cos\frac{\theta_q}{2}\sin\frac{\theta_p}{2}\right], \qquad (2.29)$$

where $p_A$, $q_A$ are the associated momentum spinors for the light-like momenta

$$\begin{aligned}
p^\mu &= p_0(1, \sin\theta_p\cos\phi_p, \sin\theta_p\sin\phi_p, \cos\theta_p), \\
q^\mu &= p_0(1, \sin\theta_q\cos\phi_q, \sin\theta_q\sin\phi_q, \cos\theta_q). \qquad (2.30)
\end{aligned}$$

The contribution $\hat{\sigma}_\gamma$ of the radiative process to the parton cross section is given by

$$\hat{\sigma}_\gamma = \frac{1}{12}\frac{1}{2s}\int \mathrm{d}\Gamma_\gamma \sum_\lambda |\mathcal{M}_\gamma^{-+-}(\lambda)|^2, \qquad (2.31)$$

where the phase-space integral is defined by

$$\int \mathrm{d}\Gamma_\gamma = \int \frac{\mathrm{d}^3\mathbf{k}_n}{(2\pi)^3 2k_{n,0}}\int \frac{\mathrm{d}^3\mathbf{k}_l}{(2\pi)^3 2k_{l,0}}\int \frac{\mathrm{d}^3\mathbf{k}}{(2\pi)^3 2k_0}(2\pi)^4\delta(p_u + p_d - k_n - k_l - k). \qquad (2.32)$$

## 2.5 Treatment of soft and collinear singularities

The phase-space integral (2.31) diverges in the soft ($k_0 \to 0$) and collinear ($p_u k, p_d k, k_l k \to 0$) regions logarithmically if the photon and fermion masses are set to zero, as done in (2.28). For the treatment of the soft and collinear singularities we applied three different methods, the results of which are in good numerical agreement. In the following we briefly sketch these approaches.

### 2.5.1 IR phase-space slicing and effective collinear factors

Firstly, we made use of the variant of phase-space slicing that is described in Ref. [35], where the soft-photon region is excluded in the integral (2.31) but the regions of photon emission collinear to the fermions are included.

In the soft-photon region $m_\gamma < k_0 < \Delta E \ll \sqrt{\hat{s}}$ the bremsstrahlung cross section factorizes into the lowest-order cross section and a universal eikonal factor that depends on the photon momentum $k$ (see, e.g., Ref. [15]). Integration over $k$ in the partonic CM frame yields a simple correction factor $\delta_{\mathrm{soft}}$ to the partonic Born cross section $\mathrm{d}\hat{\sigma}_0$,

$$\begin{aligned}
\delta_{\mathrm{soft}} = -\frac{\alpha}{2\pi}\Bigg\{ & Q_l^2\left[2\ln\Big(\frac{2\Delta E}{m_\gamma}\Big)\ln\Big(\frac{m_l^2}{\hat{s}}\Big) + 2\ln\Big(\frac{2\Delta E}{m_\gamma}\Big) + \frac{1}{2}\ln^2\Big(\frac{m_l^2}{\hat{s}}\Big) + \ln\Big(\frac{m_l^2}{\hat{s}}\Big) + \frac{\pi^2}{3}\right] \\
& + Q_d^2\left[2\ln\Big(\frac{2\Delta E}{m_\gamma}\Big)\ln\Big(\frac{m_d^2}{\hat{s}}\Big) + 2\ln\Big(\frac{2\Delta E}{m_\gamma}\Big) + \frac{1}{2}\ln^2\Big(\frac{m_d^2}{\hat{s}}\Big) + \ln\Big(\frac{m_d^2}{\hat{s}}\Big) + \frac{\pi^2}{3}\right] \\
& + Q_u^2\left[2\ln\Big(\frac{2\Delta E}{m_\gamma}\Big)\ln\Big(\frac{m_u^2}{\hat{s}}\Big) + 2\ln\Big(\frac{2\Delta E}{m_\gamma}\Big) + \frac{1}{2}\ln^2\Big(\frac{m_u^2}{\hat{s}}\Big) + \ln\Big(\frac{m_u^2}{\hat{s}}\Big) + \frac{\pi^2}{3}\right] \\
& - 2Q_lQ_d\left[2\ln\Big(\frac{2\Delta E}{m_\gamma}\Big)\ln\Big(\frac{-\hat{t}}{\hat{s}}\Big) - \mathrm{Li}_2\Big(-\frac{\hat{u}}{\hat{t}}\Big)\right] \\
& + 2Q_lQ_u\left[2\ln\Big(\frac{2\Delta E}{m_\gamma}\Big)\ln\Big(\frac{-\hat{u}}{\hat{s}}\Big) - \mathrm{Li}_2\Big(-\frac{\hat{t}}{\hat{u}}\Big)\right]\Bigg\}.
\end{aligned} \tag{2.33}$$

The factor $\delta_{\mathrm{soft}}$ can be added directly to the virtual correction factor $2\,\mathrm{Re}\{\delta^{\mathrm{virt}}\}$ defined in (2.9). It can be checked easily that the photon mass $m_\gamma$ cancels in the sum $2\,\mathrm{Re}\{\delta^{\mathrm{virt}}\}+\delta_{\mathrm{soft}}$.

The remaining phase-space integration in (2.31) with $k_0 > \Delta E$ still contains the collinear singularities in the regions in which $(p_uk)$, $(p_dk)$, or $(k_lk)$ is small. In these regions, however, the asymptotic behaviour of the differential cross section (including its dependence on the fermion masses) has a well-known form. The singular terms are universal and factorize from $\mathrm{d}\sigma_0$. A simple approach to include the collinear regions consists in a suitable modification of $|\mathcal{M}_\gamma|^2$, which was calculated for vanishing fermion masses. More precisely, $|\mathcal{M}_\gamma|^2$ is multiplied by an *effective collinear factor* that is equal to 1 up to terms of $\mathcal{O}(m_f^2/\hat{s})$ $(f = l, u, d)$ outside the collinear regions, but replaces the poles in $(p_uk)$, $(p_dk)$, and $(k_lk)$ by the correctly mass-regularized behaviour. Explicitly, the substitution reads

$$\begin{aligned}
\sum_{\lambda=\pm1} |\mathcal{M}_\gamma^{\tau_u,\tau_d,\tau_l}(\lambda)|^2 \;\to\; & \sum_{\kappa_u,\kappa_d,\kappa_l=\pm1} f_{\kappa_u}^{(\mathrm{ini})}(m_u, x_u, E_u, \theta_{u\gamma}) f_{\kappa_d}^{(\mathrm{ini})}(m_d, x_d, E_d, \theta_{d\gamma}) \\
& \times f_{\kappa_l}^{(\mathrm{fin})}(m_l, x_l, E_l, \theta_{l\gamma}) \sum_{\lambda=\pm1} |\mathcal{M}_\gamma^{\kappa_u\tau_u,\kappa_d\tau_d,\kappa_l\tau_l}(\lambda)|^2.
\end{aligned} \tag{2.34}$$

The functions $f_+^{(\mathrm{ini/fin})}$ and $f_-^{(\mathrm{ini/fin})}$ describe collinear photon emission with and without spin flip of the radiating fermion, respectively,

$$\begin{aligned}
f_+^{(\mathrm{ini/fin})}(m_f, x_f, E_f, \theta_{f\gamma}) &= \left(\frac{4E_f^2\sin^2(\theta_{f\gamma}/2)}{4E_f^2\sin^2(\theta_{f\gamma}/2) + m_f^2}\right)^2, \\
f_-^{(\mathrm{ini/fin})}(m_f, x_f, E_f, \theta_{f\gamma}) &= \frac{x_f^2}{x_f^2 \mp 2x_f + 2}\frac{4m_f^2E_f^2\sin^2(\theta_{f\gamma}/2)}{[4E_f^2\sin^2(\theta_{f\gamma}/2) + m_f^2]^2}, \qquad x_f = \frac{k_0}{E_f},
\end{aligned} \tag{2.35}$$

where $E_f$ is the fermion energy and $\theta_{f\gamma} = \angle(\mathbf{k}_f, \mathbf{k})$ is the angle of the photon emission from $f = u, d, l$.

### 2.5.2 IR and collinear phase-space slicing

Instead of using effective collinear factors, alternatively we have also applied phase-space slicing to the collinear singularities, i.e. the collinear regions are now excluded by the angular cuts $\theta_{f\gamma} < \Delta\theta \ll 1$ in the integral (2.31). The IR region is treated as previously, leading to the same correction factor $\delta_{\text{soft}}$ as given in (2.33).

In the collinear cones the photon emission angles $\theta_{f\gamma}$ can be integrated out by making use of the factorization property of the squared photon-emission matrix elements with the radiator functions $f_{\pm}^{(\text{ini/fin})}$, as described in the previous section. The resulting contribution to the bremsstrahlung cross section has the form of a convolution of the lowest-order cross section,

$$\sigma_{\text{coll}} = \sigma_{\text{coll},u} + \sigma_{\text{coll},d} + \sigma_{\text{coll},l}, \tag{2.36}$$

$$\sigma_{\text{coll},q}(p_q) = \frac{Q_q^2\alpha}{2\pi} \int_0^{1-2\Delta E/\sqrt{\hat{s}}} \mathrm{d}z \left\{ \left[ \ln\!\left(\frac{\Delta\theta^2\hat{s}}{4m_q^2}\right) - 1 \right] P_{ff}(z)\sigma_0(zp_q) + (1-z)\sigma_0(zp_q)\Big|_{\tau_q\to-\tau_q} \right\}, \qquad q = u, d, \tag{2.37}$$

$$\sigma_{\text{coll},l}(k_l) = \frac{Q_l^2\alpha}{2\pi} \int_0^{1-2\Delta E/\sqrt{\hat{s}}} \mathrm{d}z \left\{ \left[ \ln\!\left(\frac{\Delta\theta^2\hat{s}}{4m_l^2}\right) + 2\ln(z) - 1 \right] P_{ff}(z)\sigma_0(k_l) + (1-z)\sigma_0(k_l)\Big|_{\tau_l\to-\tau_l} \right\}, \tag{2.38}$$

with the splitting function

$$P_{ff}(z) = \frac{1+z^2}{1-z}. \tag{2.39}$$

For initial-state radiation the respective quark momentum $p_q$ is reduced by the factor $z$ so that the partonic CM frame for the hard scattering receives a boost, while this is not the case for final-state radiation. Note that for final-state radiation, i.e. in $\sigma_{\text{coll},l}$, the lepton momentum in the final state is $zk_l$, although $k_l$ is relevant for the lowest-order cross section in the hard scattering. Of course, if photons collinear to the lepton $l$ are not separated the $z$ integration can be carried out explicitly. It can be checked easily that in this case all logarithms of the lepton mass $m_l$ cancel in the sum of virtual and real corrections.

### 2.5.3 Subtraction method

Finally, we applied the subtraction method presented in Ref. [36], where the so-called "dipole formalism", originally introduced by Catani and Seymour [37] within massless QCD, was applied to photon radiation and generalized to massive fermions. The general idea of a subtraction method is to subtract and to add a simple auxiliary function from the singular integrand. This auxiliary function has to be chosen such that it cancels all singularities of the original integrand so that the phase-space integration of the difference

can be performed numerically. Moreover, the auxiliary function has to be simple enough so that it can be integrated over the singular regions analytically, when the subtracted contribution is added again.

The dipole subtraction function consists of contributions labelled by all ordered pairs of charged external particles, one of which is called *emitter*, the other one *spectator*. For $u\bar{d} \to \nu_l l^+$ we, thus, have six different emitter/spectator cases $ff'$: $ud$, $du$, $ul$, $lu$, $dl$, $ld$. The subtraction function that is subtracted from $\sum_\lambda |\mathcal{M}_\gamma(\lambda)|^2$ is given by

$$\begin{aligned}
|\mathcal{M}_{\rm sub}|^2 = \quad & Q_u Q_d e^2 \Big[ g_{ud}(p_u,p_d,k) |\mathcal{M}_{\rm Born}(x_{ud}p_u,p_d,k_{l,ud})|^2 \\
& \qquad + g_{du}(p_d,p_u,k) |\mathcal{M}_{\rm Born}(p_u,x_{ud}p_d,k_{l,du})|^2 \Big] \\
& - Q_u Q_l e^2 \Big[ g_{ul}(p_u,k_l,k) + g_{lu}(k_l,p_u,k) \Big] |\mathcal{M}_{\rm Born}(x_{ul}p_u,p_d,k_{l,ul})|^2 \\
& + Q_d Q_l e^2 \Big[ g_{dl}(p_d,k_l,k) + g_{ld}(k_l,p_d,k) \Big] |\mathcal{M}_{\rm Born}(p_u,x_{dl}p_d,k_{l,dl})|^2, \qquad (2.40)
\end{aligned}$$

with the functions

$$\begin{aligned}
g_{ud}(p_u,p_d,k) &= \frac{1}{(p_u k) x_{ud}} \left[ \frac{2}{1-x_{ud}} - 1 - x_{ud} \right], \\
g_{du}(p_d,p_u,k) &= \frac{1}{(p_d k) x_{ud}} \left[ \frac{2}{1-x_{ud}} - 1 - x_{ud} \right], \\
g_{ql}(p_q,k_l,k) &= \frac{1}{(p_q k) x_{ql}} \left[ \frac{2}{2-x_{ql}-z_{ql}} - 1 - x_{ql} \right], \\
g_{lu}(k_l,p_q,k) &= \frac{1}{(k_l k) x_{ql}} \left[ \frac{2}{2-x_{ql}-z_{ql}} - 1 - z_{ql} \right], \qquad q = u,d, \qquad (2.41)
\end{aligned}$$

and the auxiliary variables

$$x_{ud} = \frac{p_u p_d - p_u k - p_d k}{p_u p_d}, \qquad x_{ql} = \frac{p_q k_l + p_q k - k_l k}{p_q k_l + p_q k}, \qquad z_{ql} = \frac{p_q k_l}{p_q k_l + p_q k}. \qquad (2.42)$$

For the evaluation of $|\mathcal{M}_{\rm sub}|^2$ in (2.40) the lepton momenta $k_{l,ff'}$ still have to be specified. They are given by

$$k^\mu_{l,ud} = \Lambda(p_u,p_d)^\mu{}_\nu k_l^\nu, \qquad k^\mu_{l,du} = \Lambda(p_d,p_u)^\mu{}_\nu k_l^\nu, \qquad k^\mu_{l,ql} = k_l^\mu + k^\mu - (1-x_{ql}) p_q^\mu, \quad (2.43)$$

with the Lorentz transformation matrix

$$\Lambda(p_1,p_2)^\mu{}_\nu = g^\mu{}_\nu - \frac{(P+\tilde{P})^\mu (P+\tilde{P})_\nu}{P^2 + P\tilde{P}} + \frac{2\tilde{P}^\mu P_\nu}{P^2}, \qquad P^\mu = k_l^\mu + k_n^\mu, \quad \tilde{P}^\mu = x_{ud} p_1^\mu + p_2^\mu. \qquad (2.44)$$

The modified lepton momenta $k_{l,ff'}$ still obey the on-shell condition $k^2_{l,ff'} = 0$, and the same is true for the corresponding neutrino momenta that result from momentum conservation. It is straightforward to check that all collinear and soft singularities cancel in $\sum_\lambda |\mathcal{M}_\gamma(\lambda)|^2 - |\mathcal{M}_{\rm sub}|^2$ so that this difference can be integrated numerically over the entire phase space (2.32). If phase-space cuts are applied to the lepton momentum, these cuts directly affect $k_l$ in $\sum_\lambda |\mathcal{M}_\gamma(\lambda)|^2$, but in $|\mathcal{M}_{\rm sub}|^2$ they have to be applied to $k_{l,ff'}$. The

singularities nevertheless properly cancel in this case, since the momenta $k_{l,ff'}$ are defined in such a way that they asymptotically approach $k_l$ in the singular regions.

The contribution of $|\mathcal{M}_{\rm sub}|^2$, which has been subtracted by hand, has to be added again. This is done after the singular degrees of freedom in the phase space (2.32) are integrated out analytically, keeping an infinitesimal photon mass $m_\gamma$ and small fermion masses $m_f$ as regulators [36]. The resulting contribution is split into two parts: one that factorizes from the lowest-order cross section $\sigma_0$ and another part that has the form of a convolution integral over $\sigma_0$ with reduced CM energy. The first part is given by

$$\begin{aligned}\sigma_{\rm sub,1} = \frac{\alpha}{2\pi}\Bigg\{ & Q_u Q_d \left[\mathcal{L}(\hat{s}, m_u^2, m_d^2) + 3 - \frac{2\pi^2}{3}\right] - Q_l Q_u \left[\mathcal{L}(-\hat{u}, m_l^2, m_u^2) - \frac{1}{2} - \frac{\pi^2}{3}\right] \\ & + Q_l Q_d \left[\mathcal{L}(-\hat{t}, m_l^2, m_d^2) - \frac{1}{2} - \frac{\pi^2}{3}\right]\Bigg\}\sigma_0 + \frac{Q_l^2\alpha}{4\pi}\sigma_0\Big|_{\tau_l\to-\tau_l}\end{aligned} \tag{2.45}$$

with the auxiliary function

$$\mathcal{L}(r, m_1^2, m_2^2) = 2\ln\!\left(\frac{m_1 m_2}{r}\right)\ln\!\left(\frac{m_\gamma^2}{r}\right) + 2\ln\!\left(\frac{m_\gamma^2}{r}\right) - \frac{1}{2}\ln^2\!\left(\frac{m_1^2}{r}\right) - \frac{1}{2}\ln^2\!\left(\frac{m_2^2}{r}\right) + \ln\!\left(\frac{m_1 m_2}{r}\right). \tag{2.46}$$

The IR and fermion-mass singularities contained in $\mathrm{d}\sigma_{\rm sub,1}$ exactly cancel the ones of the virtual corrections. The second integrated subtraction contribution is given by[5]

$$\begin{aligned}\sigma_{\rm sub,2}(p_u, p_d) = {} & Q_u Q_d \frac{\alpha}{2\pi}\int_0^1 \mathrm{d}x\, \Big\{\left[\mathcal{G}_{ud}(\hat{s}, x)\right]_+ \sigma_0(xp_u, p_d) \\ & \qquad + \left[\mathcal{G}_{du}(\hat{s}, x)\right]_+ \sigma_0(p_u, xp_d)\Big\}\Big|_{\hat{s}=(p_u+p_d)^2} \\ & - Q_l Q_u \frac{\alpha}{2\pi}\int_{-\hat{s}}^0 \mathrm{d}\hat{u}\int_0^1 \mathrm{d}x\, \left[\mathcal{G}_{lu}(-\hat{u}, x)\right]_+ \frac{\mathrm{d}\sigma_0}{\mathrm{d}\hat{u}}(xp_u, p_d)\Big|_{\hat{u}=(p_d-k_n)^2} \\ & + Q_l Q_d \frac{\alpha}{2\pi}\int_{-\hat{s}}^0 \mathrm{d}\hat{t}\int_0^1 \mathrm{d}x\, \Big[\mathcal{G}_{ld}(-\hat{t}, x)\Big]_+ \frac{\mathrm{d}\sigma_0}{\mathrm{d}\hat{t}}(p_u, xp_d)\Big|_{\hat{t}=(p_u-k_n)^2} \\ & + \frac{\alpha}{2\pi}\int_0^1 \mathrm{d}x\,(1-x)\left\{Q_u^2\sigma_0(xp_u, p_d)\Big|_{\tau_u\to-\tau_u} + Q_d^2\sigma_0(p_u, xp_d)\Big|_{\tau_d\to-\tau_d}\right\},\end{aligned} \tag{2.47}$$

where the usual $[\ldots]_+$ prescription,

$$\int_0^1 \mathrm{d}x\,\Big[f(x)\Big]_+ g(x) = \int_0^1 \mathrm{d}x\, f(x)\left[g(x) - g(1)\right], \tag{2.48}$$

is applied to the integration kernels

$$\begin{aligned}\mathcal{G}_{qq'}(r, x) &= P_{ff}(x)\left[\ln\left(\frac{r}{m_q^2}\right) - 1\right], \\ \mathcal{G}_{lq}(r, x) &= P_{ff}(x)\left[\ln\left(\frac{r}{x(1-x)m_q^2}\right) - 1\right] - \frac{3}{2(1-x)}.\end{aligned} \tag{2.49}$$

[5]Note that we did not literally follow the formulae of Ref. [36], but rearranged some terms in the spin-flip parts.

In (2.47) we indicated explicitly how the Mandelstam variable $r$ has to be chosen in terms of the momenta in the evaluation of the part containing $[\mathcal{G}_{ff'}(r,x)]_+$. Note, however, that in (2.47) the variable $\hat{s}$ that is implicitly used in the calculation of $\sigma_0(\ldots)$ is reduced to $2xp_up_d$.

In summary, within the subtraction approach the real correction reads

$$\hat{\sigma}_\gamma = \frac{1}{12}\frac{1}{2s}\int \mathrm{d}\Gamma_\gamma \left[\sum_\lambda |\mathcal{M}_\gamma(\lambda)|^2 - |\mathcal{M}_{\mathrm{sub}}|^2\right] + \sigma_{\mathrm{sub},1} + \sigma_{\mathrm{sub},2}. \tag{2.50}$$

It should be realized that in $\sigma_{\mathrm{sub},1}$ and $\sigma_{\mathrm{sub},2}$ the full photonic phase space is integrated over. This does, however, not restrict the subtraction approach to observables that are fully inclusive with respect to emitted photons, but rather to observables that are inclusive with respect to photons that are soft or collinear to any charged external fermion (see discussions in Sect. 6.2 of Ref. [36] and Sect. 7 of Ref. [37]). In this context, the implementation of phase-space cuts, which define the observable, in Eq. (2.50) is crucial. The phase-space cuts have to be applied in the subtraction parts $\sigma_{\mathrm{sub},1}$, $\sigma_{\mathrm{sub},2}$, and $|\mathcal{M}_{\mathrm{sub}}|^2$, which are all defined on the $2 \to 2$ kinematics, exactly in the same way, in order to guarantee that these parts consistently cancel each other. On the other hand, the observable-defining cuts directly enter the $2 \to 3$ part $\sum_\lambda |\mathcal{M}_\gamma(\lambda)|^2$. Consistency requires that these cuts treat soft or collinear photons inclusively, i.e. that photons collinear to charged fermions have to be associated with these fermions; otherwise $|\mathcal{M}_{\mathrm{sub}}|^2$ cannot locally cancel the collinear singularities in $\sum_\lambda |\mathcal{M}_\gamma(\lambda)|^2$.

# 3 The hadronic processes $\mathrm{pp}, \mathrm{p\bar{p}} \to \mathrm{W}^+ \to l^+\nu_l(+\gamma)$

The proton–(anti-)proton cross section $\sigma$ is obtained from the parton cross sections $\hat{\sigma}^{(q_1q_2)}$ by convolution with the corresponding parton distribution functions $q_{1,2}(x)$,

$$\sigma(s) = \sum_{q_1q_2}\int_0^1 \mathrm{d}x_1 \int_0^1 \mathrm{d}x_2\, q_1(x_1)q_2(x_2)\hat{\sigma}^{(q_1q_2)}(x_1p_{q_1}, x_2p_{q_2}). \tag{3.1}$$

In the sum $\sum_{q_1q_2}$ the quark pairs $q_1q_2$ run over all possible combinations $u\bar{d}$ and $\bar{d}u$ of up-type quarks $u = \mathrm{u}, \mathrm{c}$ and down-type quarks $d = \mathrm{d}, \mathrm{s}$. The squared CM energy $s$ of the pp ($\mathrm{p\bar{p}}$) system is related to the squared parton CM energy $\hat{s}$ by $\hat{s} = x_1x_2s$.

The $\mathcal{O}(\alpha)$-corrected parton cross section $\hat{\sigma}^{(q_1q_2)}$ contains mass singularities of the form $\alpha\ln(m_q)$, which are due to collinear photon radiation off the initial-state quarks. In complete analogy to the $\overline{\mathrm{MS}}$ factorization scheme for next-to-leading order QCD corrections, we absorb these collinear singularities into the quark distributions. This is achieved by replacing $q(x)$ in (3.1) according to

$$q(x) \to q(x,M^2) - \int_x^1 \frac{\mathrm{d}z}{z}\, q\Big(\frac{x}{z}, M^2\Big)\, \frac{\alpha}{2\pi}\, Q_q^2 \left[P_{ff}(z)\Big\{\ln\Big(\frac{M^2}{m_q^2}\Big) - 2\ln(1-z) - 1\Big\}\right]_+, \tag{3.2}$$

where $M$ is the factorization scale. This replacement defines the same finite parts in the $\mathcal{O}(\alpha)$ correction as the usual $\overline{\mathrm{MS}}$ factorization in $D$-dimensional regularization for exactly massless partons, where the $\ln(m_q)$ terms appear as $1/(D-4)$ poles. In (3.2) we have

preferred to exclude the soft-photon pole by using the $[\ldots]_+$ prescription. This procedure is fully equivalent to the application of a soft-photon cutoff, as used in Ref. [8].

The absorption of the collinear singularities of $\mathcal{O}(\alpha)$ into quark distributions, as a matter of fact, requires also the inclusion of the corresponding $\mathcal{O}(\alpha)$ corrections into the DGLAP evolution of these distributions and into their fit to experimental data. At present, this full incorporation of $\mathcal{O}(\alpha)$ effects in the determination of the quark distributions has not yet been performed. However, an approximate inclusion of the $\mathcal{O}(\alpha)$ corrections to the DGLAP evolution shows [38] that the impact of these corrections on the quark distributions is well below 1%, at least in the $x$ range that is relevant for W-boson production at the Tevatron and the LHC. Therefore, the neglect of these corrections to the parton distributions is justified for the following numerical study.

# 4 Numerical results

## 4.1 Input parameters

For the numerical evaluation we used the following set of parameters,

$$
\begin{array}{llll}
\alpha = 1/137.0359895, & \alpha(M_{\mathrm{Z}}^2) = 1/128.887, & G_\mu = 1.16637 \times 10^{-5}\,\mathrm{GeV}^{-2}, \\
M_{\mathrm{W}} = 80.35\,\mathrm{GeV}, & M_{\mathrm{Z}} = 91.1867\,\mathrm{GeV}, & M_{\mathrm{H}} = 150\,\mathrm{GeV}, \\
\Gamma_{\mathrm{W}} = 2.08699\ldots\,\mathrm{GeV}, & \alpha_{\mathrm{s}} = 0.119, & \\
m_{\mathrm{e}} = 0.51099907\,\mathrm{MeV}, & m_\mu = 105.658389\,\mathrm{MeV}, & m_\tau = 1.77705\,\mathrm{GeV}, \\
m_{\mathrm{u}} = 4.85\,\mathrm{MeV}, & m_{\mathrm{c}} = 1.55\,\mathrm{GeV}, & m_{\mathrm{t}} = 174.17\,\mathrm{GeV}, \\
m_{\mathrm{d}} = 4.85\,\mathrm{MeV}, & m_{\mathrm{s}} = 150\,\mathrm{MeV}, & m_{\mathrm{b}} = 4.5\,\mathrm{GeV}, \\
|V_{\mathrm{ud}}| = 0.975, & |V_{\mathrm{us}}| = 0.222, & \\
|V_{\mathrm{cd}}| = 0.222, & |V_{\mathrm{cs}}| = 0.975, &
\end{array}
\tag{4.1}
$$

which is consistent with experimental data [39]. Except for the CKM matrix elements, this input is identical with the one used in the LEP2 Monte Carlo workshop report [29] on precision calculations for LEP2.

We recall that the above set of data is overcomplete, but all the numbers are needed for the evaluation of the $\mathcal{O}(\alpha)$ corrected cross section in the different input schemes described in Sect. 2.1. The masses of the light quarks are only relevant for the evaluation of the charge renormalization constant $\delta Z_e$, which drops out in the $\alpha(M_{\mathrm{Z}})$- and $G_\mu$-schemes; the values for these masses are adjusted to reproduce the hadronic contribution to the photonic vacuum polarization [18]. The value for the W-boson decay width $\Gamma_{\mathrm{W}}$ is the $\mathcal{O}(\alpha)$- and $\mathcal{O}(\alpha_{\mathrm{s}})$-corrected SM prediction in the $G_\mu$ scheme. Note that $\alpha_{\mathrm{s}}$ only enters the calculation of $\Gamma_{\mathrm{W}}$ in the results presented here, since we do not consider QCD corrections to the scattering processes. If not stated otherwise, the presented cross sections and distributions are calculated for a fixed W-boson width. We consistently take the CTEQ4L [40] quark distributions for the evaluation of the pp and $\mathrm{p\bar{p}}$ cross sections. If not stated otherwise the factorization scale $M$ is set to the W-boson mass $M_{\mathrm{W}}$, which is the standard

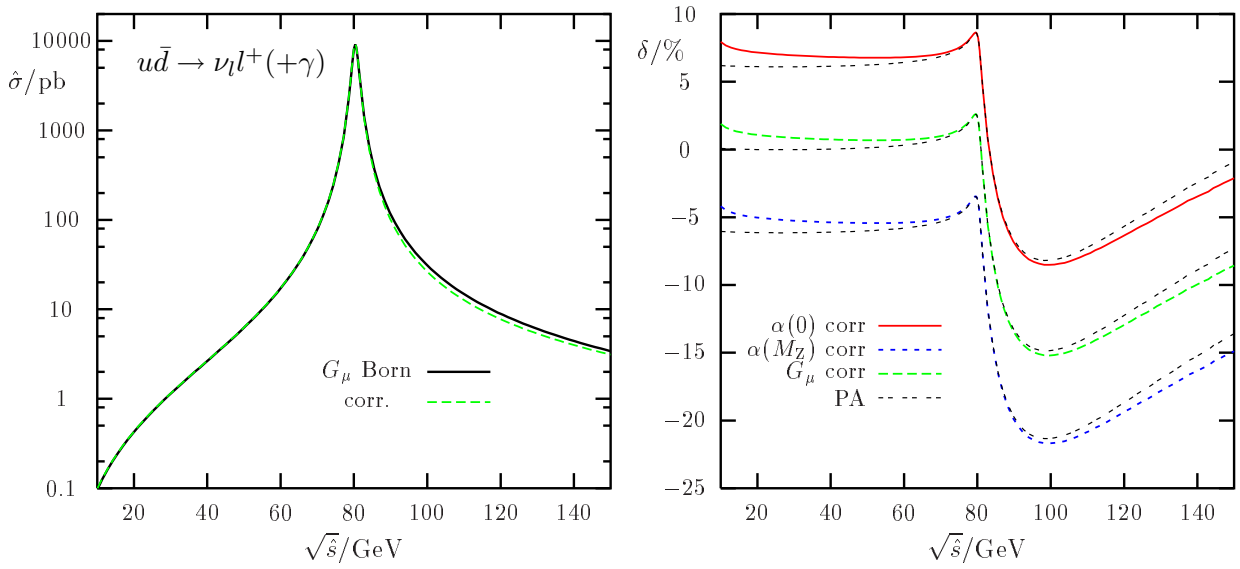


Figure 6: Total parton cross section $\hat{\sigma}$ in $G_\mu$ parametrization and relative corrections $\delta$ for different parametrizations; the respective PAs for $\delta$ are shown for comparison.

| $\sqrt{\hat{s}}$/GeV | 40 | 80 | 120 | 200 | 500 | 1000 | 2000 |
|---|---|---|---|---|---|---|---|
| $\hat{\sigma}_0$/pb | 2.646 | 7991.4 | 8.906 | 1.388 | 0.165 | 0.0396 | 0.00979 |
| $\delta$/% | 0.7 | 2.42 | −12.9 | −3.3 | 12 | 19 | 23 |
| $\delta_{\mathrm{PA}}$/% | 0.0 | 2.40 | −12.3 | −0.7 | 18 | 31 | 43 |

Table 1: Total lowest-order parton cross section $\hat{\sigma}_0$ in $G_\mu$ parametrization and corresponding relative correction $\delta$, exact and in PA.

choice for resonant W production. A thorough investigation of the full QCD and QED factorization scale dependence would require the inclusion of the relevant QCD corrections and QED-improved parton densities, which is beyond the scope of this paper. Instead we at least study the dependence of the $\mathcal{O}(\alpha)$-corrected hadron cross sections on the QED factorization scale $M$ using parton densities without QED evolution.

## 4.2 Results for the parton process

Figure 6 shows the total partonic cross section $\hat{\sigma}$ and the corresponding relative correction $\delta$ for intermediate energies. Note that the total cross section (including its correction) is the same for all final-state leptons $l = \mathrm{e}, \mu, \tau$ in the limit of vanishing lepton masses. As expected, the $G_\mu$ parametrization of the Born cross section minimizes the correction at low energies, since the universal corrections induced by the running of $\alpha$ and by the $\rho$ parameter are absorbed in the lowest-order cross section. Moreover, the naive error estimate (2.25) for the PA turns out to be realistic. The PA describes the correction in the resonance region within a few 0.1%. Table 1 contains some results on the partonic cross section and its correction up to energies in the TeV range. Far above resonance the

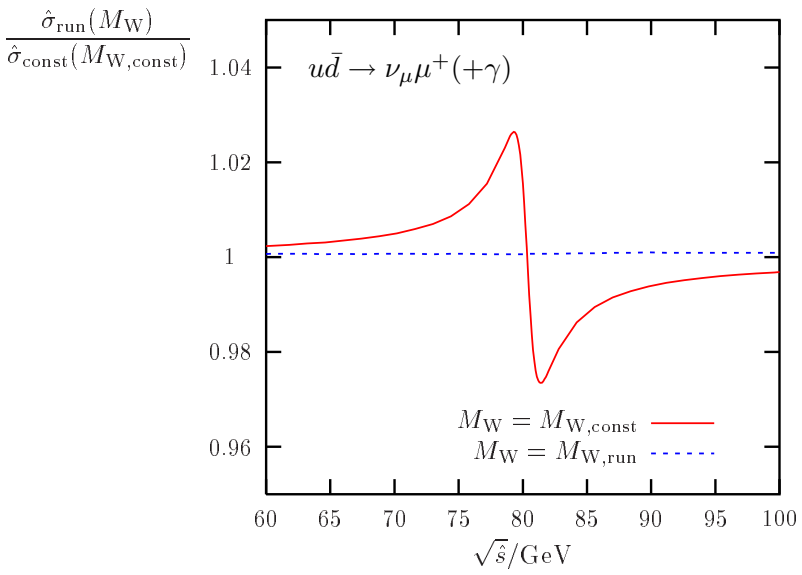


Figure 7: Ratio of $u\bar{d} \to \nu_\mu \mu^+(+\gamma)$ cross sections in the $G_\mu$-scheme evaluated with running and constant widths in the W propagator.

PA cannot describe the exact correction anymore, since non-resonant corrections become more and more important. The difference between the full $\mathcal{O}(\alpha)$ correction and the PA is mainly due to (negative) Sudakov logarithms of the form $\alpha \ln^2(\hat{s}/M_{\rm W}^2)$, which are not contained in the PA, but in the full $\mathcal{O}(\alpha)$ correction. The large positive correction at high energies is induced by the radiative return to the W resonance via photon emission from the initial-state quarks and from the W boson, i.e. the reaction proceeds as W$\gamma$ production with subsequent W decay in this case.

Finally, we investigate the relation between the parametrizations of the W resonance by a constant or running width. As explained in Sect. 2.1, at tree level the transition from a running to a constant width in the cross section is equivalent to the change (2.6) in $M_{\rm W}$ and $\Gamma_{\rm W}$. Here we check whether, or to which accuracy, this statement remains valid in the presence of the $\mathcal{O}(\alpha)$ corrections. Figure 7 shows the ratio $\hat{\sigma}_{\rm run}/\hat{\sigma}_{\rm const}$ of the cross sections for $u\bar{d} \to \nu_\mu \mu^+(+\gamma)$, evaluated with a running width ($\hat{\sigma}_{\rm run}$) and with a constant width ($\hat{\sigma}_{\rm const}$). Switching from one parametrization to the other without correcting $M_{\rm W}$ and $\Gamma_{\rm W}$ changes the cross section at the level of a few per cent near the resonance, as expected. However, adjusting additionally $M_{\rm W}$ and $\Gamma_{\rm W}$ according to (2.6), absorbs this change in the cross section up to a difference that is below 0.1%. This means that also in the presence of the $\mathcal{O}(\alpha)$ corrections the results of a W-mass or width determination can be transformed from one parametrization to the other via (2.6), without repeating the analysis in the other parametrization.

The results of this section have been obtained with the three variants described in Sect. 2.5 for combining virtual and real corrections. For slicing parameters $2\Delta E/\sqrt{\hat{s}}$ and $\Delta\theta$ in the range $10^{-3}$–$10^{-5}$ the results agree within the integration errors, which are significantly below the accuracy of the numbers in Table 1.

## 4.3 Results for $pp \to W^+ \to \nu_l l^+(+\gamma)$ at the LHC

We first consider W production at the LHC, i.e. we assume a pp initial state with a CM energy of $\sqrt{s} = 14\,\text{TeV}$. For the experimental identification of the process $pp \to W^+ \to \nu_l l^+(+\gamma)$ we take the set of phase space cuts

$$p_{T,l} > 25\,\text{GeV}, \qquad \not{p}_T > 25\,\text{GeV}, \qquad |\eta_l| < 1.2, \tag{4.2}$$

where $p_{T,l}$ and $\eta_l$ are the transverse momentum and the rapidity of the charged lepton $l^+$, respectively, and $\not{p}_T = p_{T,\nu_l}$ is the missing transverse momentum carried away by the neutrino. Note that these cuts are not "collinear-safe" with respect to the lepton momentum, so that observables in general receive corrections that involve large lepton-mass logarithms of the form $\alpha \ln(m_l/M_W)$. This is due to the fact that photons within a small collinear cone around the charged lepton momentum are not treated inclusively, i.e. the cuts assume a perfect isolation of photons from the charged lepton. While this is (more or less) achievable for muon final states, it is not realistic for electrons. In order to be closer to the experimental situation for electrons, we additionally consider the following photon recombination procedure:

1. Photons with a rapidity $|\eta_\gamma| > 2.5$, which are close to the beams, are treated as invisible, i.e. they are considered as part of the proton remnant.

2. If the photon survived the first step, and if the resolution $R_{l\gamma} = \sqrt{(\eta_l - \eta_\gamma)^2 + \phi_{l\gamma}^2}$ is smaller than 0.1 (with $\phi_{l\gamma}$ denoting the angle between lepton and photon in the transverse plane), then the photon is recombined with the charged lepton, i.e. the momentum of the photon and $l$ are added and associated with the momentum of $l$, and the photon is discarded.

3. Finally, all events are discarded in which the resulting momentum of the charged lepton does not pass the cuts given in (4.2).

While the electroweak corrections differ for final-state electrons and muons without photon recombination, called "bare" leptons in the following, the corrections become universal in the presence of photon recombination, since the lepton-mass logarithms cancel in this case, in accordance with the KLN theorem [41]. From the explanations at the end of Sect. 2.5.3 it is clear that the described subtraction approach is not applicable without photon recombination, i.e. for bare leptons, while the slicing variants can be used with and without photon recombination.

Figures 8 and 9 show the distributions in the transverse-momentum $p_{T,l}$ and in the transverse-invariant-mass $M_{T,\nu_l l}$ in $pp \to W^+ \to \nu_l l^+(+\gamma)$ for the LHC energy, together with the corresponding relative electroweak corrections $\delta$. The transverse-invariant-mass is defined by $M_{T,\nu_l l} = \sqrt{2 p_{T,l} \not{p}_T (1 - \cos\phi_{\nu_l l})}$, where $\phi_{\nu_l l}$ is the angle between the lepton and the missing momentum in the transverse plane. The distributions show the well-known kinks at $p_{T,l} \approx M_W/2$ and $M_{T,\nu_l l} \approx M_W$, which are used in the W-mass determination. Near these kinks the correction $\delta$ reaches the order of 10–20% for bare leptons, where the larger corrections occur in the electron case, because the logarithm $\alpha \ln(m_l/M_W)$ is larger in this case. Since these enhanced corrections originate from collinear final-state radiation,

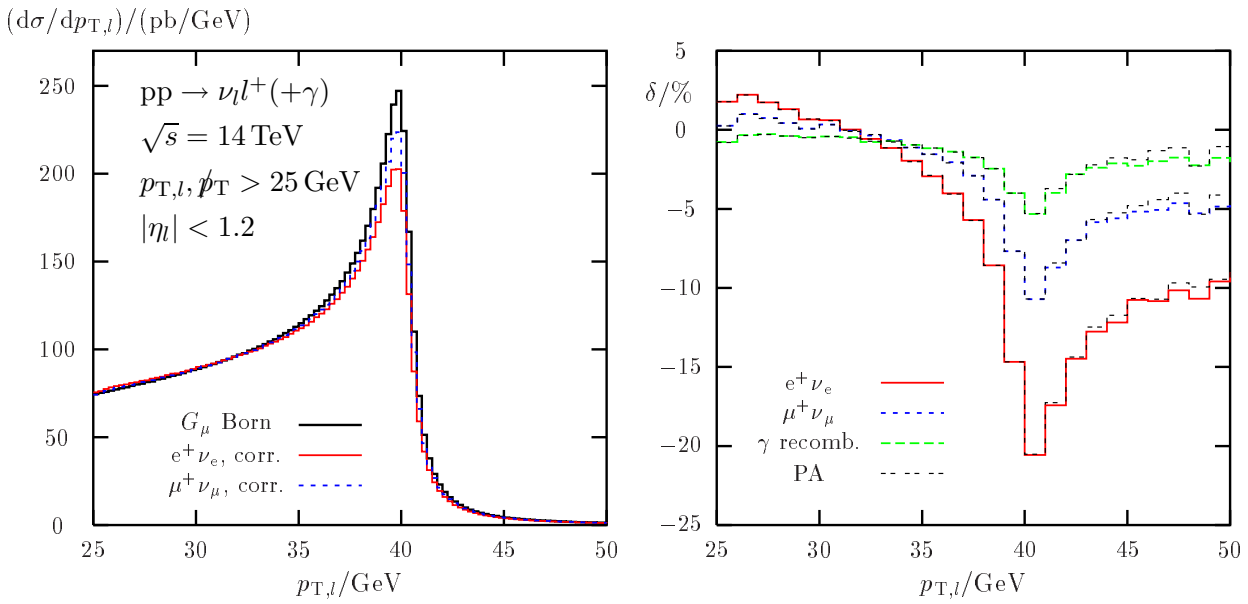


Figure 8: Transverse-momentum distribution ($d\sigma/dp_{\mathrm{T},l}$) and relative corrections $\delta$.

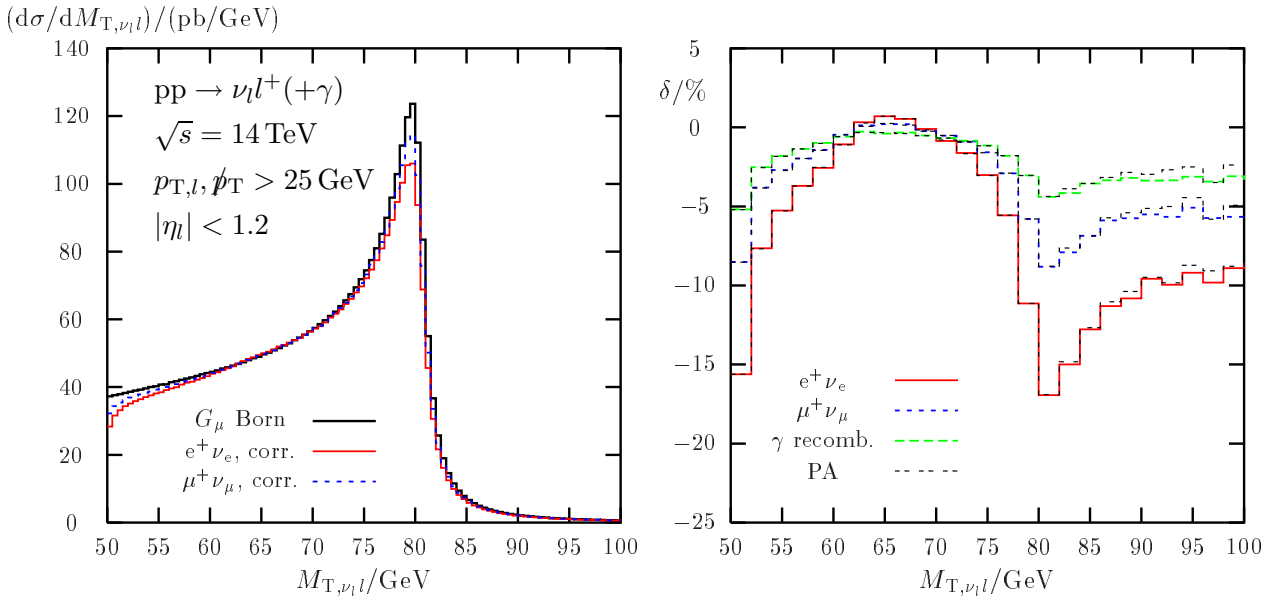


Figure 9: Transverse-invariant-mass distribution ($d\sigma/dM_{\mathrm{T},\nu_l l}$) and relative corrections $\delta$.

| $pp \to \nu_l l^+(+\gamma)$ at $\sqrt{s} = 14\,\text{TeV}$ | | | | | | |
|---|---|---|---|---|---|---|
| $p_{\text{T},l}$/GeV | 25–$\infty$ | 50–$\infty$ | 100–$\infty$ | 200–$\infty$ | 500–$\infty$ | 1000–$\infty$ |
| $\sigma_0$/pb | 1933.5(3) | 11.50(1) | 0.8198(4) | 0.1015(1) | 0.005277(1) | 0.0003019(1) |
| $\delta_{e^+\nu_e}$/% | −5.5(1) | −9.2(1) | −11.8(1) | −16.5(1) | −27.5(2) | −39.1(1) |
| $\delta_{e^+\nu_e,\text{PA}}$/% | −5.4(1) | −8.0(1) | −7.3(1) | −7.8(1) | −10.3(2) | −13.0(1) |
| $\delta_{\mu^+\nu_\mu}$/% | −2.9(1) | −4.9(1) | −8.5(1) | −13.1(1) | −23.4(1) | −34.5(1) |
| $\delta_{\mu^+\nu_\mu,\text{PA}}$/% | −2.8(1) | −3.5(1) | −4.0(1) | −4.4(1) | −6.2(1) | −8.5(1) |
| $\delta_{\text{rec}}$/% | −1.8(1) | −2.7(1) | −6.2(1) | −10.2(1) | −19.6(1) | −29.6(1) |
| $\delta_{\text{rec,PA}}$/% | −1.8(1) | −1.5(1) | −1.6(1) | −1.6(1) | −2.4(1) | −3.6(1) |
| $\Delta(2^{\pm1}M_{\text{W}})$/% | ±0.1 | ±0.1 | ±0.1 | ±0.1 | ±0.1 | ±0.2 |
| $\Delta(M_{\text{T},\nu_l l})$/% | −0.0 | 0.0 | 0.1 | 0.2 | 0.5 | 0.8 |

Table 2: Integrated lowest-order pp cross sections $\sigma_0$ for different ranges in $p_{\text{T},l}$ and corresponding relative corrections $\delta$, exact and in PA. The QED scale uncertainty is illustrated by $\Delta(M)$, as described in the text.

they are negative for higher $p_{\text{T},l}$ and redistribute events to lower transverse momenta. The correction $\delta$ is reduced to a few per cent after photon recombination, which eliminates the artificial lepton-mass logarithms.

Moreover, Figures 8 and 9 demonstrate the reliability of the PA for transverse lepton momenta $p_{\text{T},l} \lesssim M_{\text{W}}/2$, where resonant W bosons dominate. The PA curves are included in the plots as thin double-dashed lines close to the corresponding full corrections. Only for transverse momenta above the resonance region a systematic difference between the PA and the full result starts to become apparent.

Transverse lepton momenta $p_{\text{T},l}$ above the resonance kink need to be considered for the determination of the W decay width $\Gamma_{\text{W}}$ and, in the high-energy tail, for searches for new physics, such as new W′ gauge bosons. Table 2 shows the high-$p_{\text{T},l}$ contributions to the total cross section defined by different ranges in $p_{\text{T},l}$. Although the cross section rapidly decreases for high $p_{\text{T},l}$, sizeable event numbers can be expected for $p_{\text{T},l}$ values in the range 100–1000 GeV at the LHC. The results of Table 2 reveal that the PA is not applicable for very large $p_{\text{T},l}$, where the W boson is far off shell. This fact was also to be expected from the results at the parton level discussed in the previous section. As mentioned previously, the breakdown of the PA is mainly due to the missing Sudakov logarithms, which are independent of the lepton species. This explains why the PA breaks down both for electrons and muons in the same way, with or without photon recombination. Moreover, these large negative corrections of up to $\sim 30\%$ for $p_{\text{T},l}$ values between 500–1000 GeV do not become small after photon recombination. Note also that the large positive correction to the total parton cross section at high scattering energies (see Table 1), which is mainly due to resonant $W\gamma$ production in the forward and backward directions, is widely suppressed

at the hadron level. The reason for this suppression is the cut on the transverse lepton momentum which effectively demands large W momenta.

Table 2 additionally shows the uncertainty of the $\mathcal{O}(\alpha)$-corrected cross sections that is due to the dependence on the QED factorization scale $M$, as described in Sect. 3. The quantity

$$\Delta(M) = \delta(M) - \delta \tag{4.3}$$

quantifies the difference of the relative correction $\delta(M)$, evaluated for the scale $M$, to its value $\delta$ for the default choice $M = M_{\mathrm{W}}$. This difference $\Delta(M)$ applies to each row in Table 2, since the $M$-dependent part is the same for each version of $\delta_{\dots}$ shown in the table. We have chosen the values $M = 2^{\pm 1} M_{\mathrm{W}}$ and $M = M_{\mathrm{T},\nu_l l}$ for illustration, the former representing a simple rescaling of our default choice, the latter a scale choice that might be more appropriate for large transverse momenta. Although the parton densities have not been corrected for the QED factorization (see Sect. 3), the QED scale dependence turns out to be negligible compared to the other theoretical uncertainties and the expected experimental accuracy. Using QED-improved parton densities the QED factorization scale dependence should be reduced further.

The results without photon recombination have been obtained with the two slicing variants of Sect. 2.5 with the same values for the cut parameters as at the parton level. The results with photon recombination have also been checked with the subtraction approach. For the distributions shown in Figs. 8 and 9, the results from the different methods agree at the level of the line width in the plots.[6] The results of Table 2 have been obtained with the various methods with an agreement within 1–2 standard deviations, apart from a few exceptions due to fluctuations (signalled by a large $\chi^2$/d.o.f.). Apart from those, all numbers without photon recombination result from the "effective collinear factor" approach, while the ones with photon recombination are obtained with subtraction.

## 4.4 Results for $\mathrm{p\bar{p}} \to \mathrm{W}^+ \to \nu_l l^+(+\gamma)$ at the Tevatron

Now we consider W production at the Tevatron, i.e. at a $\mathrm{p\bar{p}}$ collider with a CM energy of $\sqrt{s} = 2\,\mathrm{TeV}$. We again use the phase space of (4.2) and the photon recombination procedure[7] of the previous section.

The corrections to the transverse-momentum and transverse-invariant-mass distributions at intermediate transverse momenta, displayed in Figs. 10 and 11, are of the same size as the ones discussed for the LHC in the previous section. They also show the same qualitative features under the changes in the lepton mass and after photon recombination. Moreover, the results for the PA are again not distinguishable from the full correction in

[6] Of course, the statistical error of the histogram bins is somewhat larger than the line width, at least for large transverse momenta and invariant masses. This means that the differences between the subtraction and slicing variants are even smaller than the statistical error. However, this simply results from the fact that in all cases the same set of random numbers was used, which introduces correlations among the statistical errors in the contributions that are not affected by subtraction or slicing.

[7] More realistic electron and muon identification procedures for the Tevatron have been used in Ref. [8], where electroweak corrections to the transverse momentum and invariant-mass distributions have been evaluated in another variant of the pole approximation.

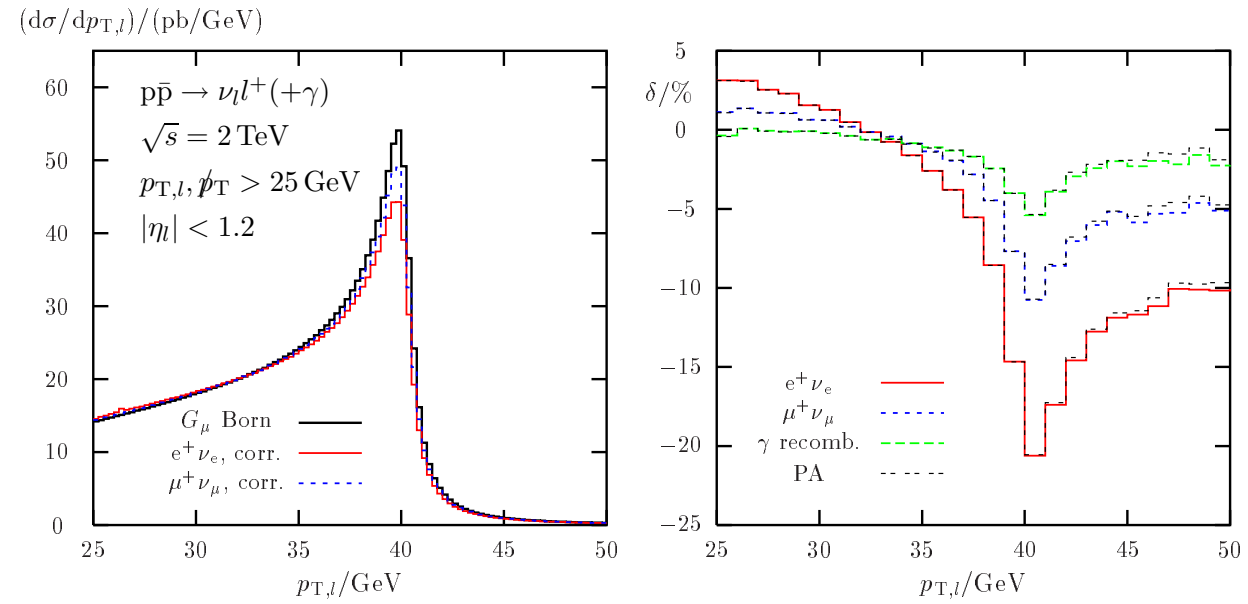


Figure 10: Transverse-momentum distribution ($d\sigma/dp_{\mathrm{T},l}$) and relative corrections $\delta$.

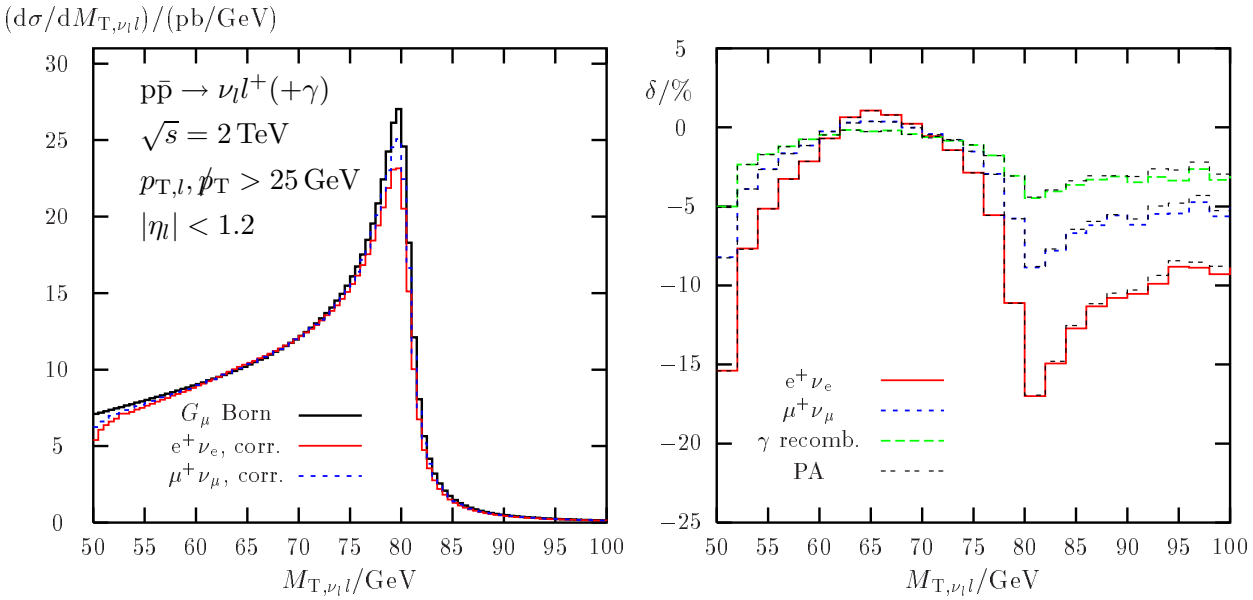


Figure 11: Transverse-invariant-mass distribution ($d\sigma/dM_{\mathrm{T},\nu_l l}$) and relative corrections $\delta$.

| $p\bar{p} \to \nu_l l^+(+\gamma)$ at $\sqrt{s} = 2\,\text{TeV}$ | | | | | | |
|---|---|---|---|---|---|---|
| $p_{\text{T},l}$/GeV | 25–$\infty$ | 50–$\infty$ | 75–$\infty$ | 100–$\infty$ | 200–$\infty$ | 300–$\infty$ |
| $\sigma_0$/pb | 407.03(5) | 2.481(1) | 0.3991(1) | 0.1305(1) | 0.006020(2) | 0.0004821(1) |
| $\delta_{e^+\nu_e}$/% | −5.4(1) | −9.7(1) | −11.2(1) | −12.9(1) | −18.8(1) | −23.8(1) |
| $\delta_{e^+\nu_e,\text{PA}}$/% | −5.3(1) | −8.6(1) | −8.7(1) | −9.2(1) | −11.7(1) | −14.1(1) |
| $\delta_{\mu^+\nu_\mu}$/% | −2.9(1) | −5.3(1) | −7.3(1) | −9.0(1) | −14.2(1) | −18.5(1) |
| $\delta_{\mu^+\nu_\mu,\text{PA}}$/% | −2.8(1) | −4.2(1) | −4.8(1) | −5.2(1) | −7.1(1) | −8.8(1) |
| $\delta_{\text{rec}}$/% | −1.8(1) | −2.7(1) | −4.8(1) | −6.3(1) | −10.4(1) | −13.6(1) |
| $\delta_{\text{rec,PA}}$/% | −1.7(1) | −1.6(1) | −2.3(1) | −2.5(1) | −3.3(1) | −3.9(1) |
| $\Delta(2^{\pm1}M_{\text{W}})$/% | ±0.1 | ±0.1 | ±0.1 | ±0.1 | ±0.2 | ±0.2 |
| $\Delta(M_{\text{T},\nu_l l})$/% | −0.0 | 0.1 | 0.1 | 0.2 | 0.5 | 0.7 |

Table 3: Integrated lowest-order $p\bar{p}$ cross sections $\sigma_0$ for different ranges in $p_{\text{T},l}$ and corresponding relative corrections $\delta$, exact and in PA. The QED scale uncertainty is illustrated by $\Delta(M)$, as described in thet text.

the plots as long as resonant W production is possible; only for transverse momenta $p_{\text{T},l}$ much larger than $M_{\text{W}}/2$ differences become visible.

The corrections to the high-transverse momentum tail are illustrated in Table 3. As expected, the PA again becomes worse with increasing $p_{\text{T},l}$, but owing to the lower luminosity and the smaller cross section at the Tevatron in comparison to the LHC it will be extremely hard to see any effect of the enhanced electroweak corrections at high $p_{\text{T},l}$. Concerning the QED factorization scale dependence, which is again quantified by $\Delta(M)$, the same remarks apply that have already been made for the LHC case. The QED scale uncertainty turns out to be negligible.

# 5 Conclusions

We have calculated the complete set of electroweak $\mathcal{O}(\alpha)$ corrections to the Drell–Yan-like W-boson production at hadron colliders. Particular attention has been paid to issues of gauge invariance and the instability of the W bosons. All relevant formulae are listed in a form that facilitates their implementation in computer codes. Besides results for the full correction for off-shell W bosons, we have also presented an expansion of the virtual correction about the W-resonance pole, which is considerably simpler than the full result.

Numerical results have been discussed at the parton level and for hadronic collisions at the LHC and at the Tevatron. The electroweak corrections significantly influence the transverse momentum and invariant-mass distributions of the decay leptons that are used in the determination of the W-boson mass. The pole approximation yields a good description of the corrections to these observables. This result justifies, in particular, the

present practice at the Tevatron, where such an approximation is used in the W-mass measurement. However, in the domains of non-resonant W-boson production in these distributions, which are relevant for the measurement of the W-boson width or for the search of new-physics effects at the LHC, this approximation fails, rendering the complete correction important; the $\mathcal{O}(\alpha)$ corrections reduce the signal by several 10% for transverse lepton momenta with $p_{\mathrm{T},l} \gtrsim 100\,\mathrm{GeV}$. To further improve the analysis, in particular in the large-$p_{\mathrm{T}}$ domain, more theoretical studies of electroweak higher-order effects as well as realistic experimental simulations are desirable.

### Note added

While this paper was completed, another calculation of the electroweak $\mathcal{O}(\alpha)$ corrections to W production, including non-resonant contributions, has been presented in Ref. [42]. The numerical results mainly focus on observables measured at RHIC, but also include the transverse lepton momentum distribution at the Tevatron. However, no mass factorization has been performed in Ref. [42], so that the corrections depend very sensitively on the light quark masses. A direct comparison with the numerical results presented in our paper is thus not possible.


## Acknowledgement

We would like to thank U. Baur, M. Dittmar, W. Hollik, H. Spiesberger, and D. Wackeroth for helpful discussions. This work has been supported in part by the European Union under contract HPRN-CT-2000-00149.


# Appendix

## A Vertex and box corrections

### A.1 Form factor for the $Wff'$ vertex

The form factor $F_{Wff'}(\hat{s})$ used in (2.12) for the vertex corrections is explicitly given by

$$
\begin{aligned}
F_{Wff'}(\hat{s}) = \frac{\alpha}{16\pi}\Bigg\{ & \frac{2(1-2s_{\mathrm{W}}^2-4Q_fQ_{f'}s_{\mathrm{W}}^2)}{c_{\mathrm{W}}^2 s_{\mathrm{W}}^2} + \frac{4}{s_{\mathrm{W}}^2}\biggl(2+\frac{M_{\mathrm{W}}^2}{\hat{s}}\biggr)B_0(0,0,M_{\mathrm{W}}) \\
& + \frac{2}{c_{\mathrm{W}}^2 s_{\mathrm{W}}^2}(1-2s_{\mathrm{W}}^2+2Q_f^2 s_{\mathrm{W}}^4+2Q_{f'}^2 s_{\mathrm{W}}^4)\biggl(2+\frac{M_{\mathrm{Z}}^2}{\hat{s}}\biggr)B_0(0,0,M_{\mathrm{Z}}) \\
& - 4\biggl(1+\frac{M_{\mathrm{W}}^2}{\hat{s}}\biggr)B_0(\hat{s},0,M_{\mathrm{W}}) - \frac{4c_{\mathrm{W}}^2}{s_{\mathrm{W}}^2}\biggl(1+\frac{M_{\mathrm{W}}^2+M_{\mathrm{Z}}^2}{\hat{s}}\biggr)B_0(\hat{s},M_{\mathrm{W}},M_{\mathrm{Z}}) \\
& + \frac{1}{c_{\mathrm{W}}^2 s_{\mathrm{W}}^2}\biggl[2\frac{M_{\mathrm{Z}}^2}{\hat{s}}(Q_f-Q_{f'}-2Q_f s_{\mathrm{W}}^2)(Q_f-Q_{f'}+2Q_{f'}s_{\mathrm{W}}^2) \\
& \quad + 3(1-2s_{\mathrm{W}}^2-4Q_fQ_{f'}s_{\mathrm{W}}^2)\biggr]B_0(\hat{s},0,0)
\end{aligned}
$$

$$
\begin{aligned}
&+ 8Q_f^2 B_0(m_f^2, 0, m_f) + 8Q_{f'}^2 B_0(m_{f'}^2, 0, m_{f'}) \\
&- 8Q_f Q_{f'} \hat{s} C_0(m_f^2, m_{f'}^2, \hat{s}, m_f, m_\gamma, m_{f'}) \\
&+ 8Q_f(Q_f - Q_{f'}) M_\mathrm{W}^2 C_0(m_f^2, 0, \hat{s}, 0, m_f, M_\mathrm{W}) \\
&- 8Q_{f'}(Q_f - Q_{f'}) M_\mathrm{W}^2 C_0(m_{f'}^2, 0, \hat{s}, 0, m_{f'}, M_\mathrm{W}) \\
&+ \frac{8c_\mathrm{W}^2}{s_\mathrm{W}^2}\Big(M_\mathrm{W}^2 + M_\mathrm{Z}^2 + \frac{M_\mathrm{W}^2 M_\mathrm{Z}^2}{\hat{s}}\Big) C_0(0, 0, \hat{s}, M_\mathrm{W}, 0, M_\mathrm{Z}) \\
&+ \frac{2}{c_\mathrm{W}^2 s_\mathrm{W}^2}(Q_f - Q_{f'} - 2Q_f s_\mathrm{W}^2)(Q_f - Q_{f'} + 2Q_{f'} s_\mathrm{W}^2) \\
&\quad \times \Big(1 + \frac{M_\mathrm{Z}^2}{\hat{s}}\Big)^2 \hat{s} C_0(0, 0, \hat{s}, 0, M_\mathrm{Z}, 0)\Big\}, \qquad \text{(A.1)}
\end{aligned}
$$

where the weak isospins $I^3_{\mathrm{W},f}$ and $I^3_{\mathrm{W},f'}$ of the fermions are implicitly taken to be $Q_f - Q_{f'} = 2I^3_{\mathrm{W},f} = -2I^3_{\mathrm{W},f'}$. Here and in the following the scalar integrals $B_0$, $C_0$, and $D_0$ depend on their arguments as follows,

$$
\begin{aligned}
&B_0(p_1^2, m_0, m_1) = \frac{(2\pi\mu)^{4-D}}{\mathrm{i}\pi^2} \int \mathrm{d}^D q \frac{1}{[q^2 - m_0^2 + \mathrm{i}\epsilon][(q+p_1)^2 - m_1^2 + \mathrm{i}\epsilon]}, \\
&C_0(p_1^2, (p_2-p_1)^2, p_2^2, m_0, m_1, m_2) = \frac{1}{\mathrm{i}\pi^2} \int d^4 q \\
&\quad \times \frac{1}{[q^2 - m_0^2 + \mathrm{i}\epsilon][(q+p_1)^2 - m_1^2 + \mathrm{i}\epsilon][(q+p_2)^2 - m_2^2 + \mathrm{i}\epsilon]}, \\
&D_0(p_1^2, (p_2-p_1)^2, (p_3-p_2)^2, p_3^2, p_2^2, (p_3-p_1)^2, m_0, m_1, m_2, m_3) = \frac{1}{\mathrm{i}\pi^2} \int d^4 q \\
&\quad \times \frac{1}{[q^2 - m_0^2 + \mathrm{i}\epsilon][(q+p_1)^2 - m_1^2 + \mathrm{i}\epsilon][(q+p_2)^2 - m_2^2 + \mathrm{i}\epsilon][(q+p_3)^2 - m_3^2 + \mathrm{i}\epsilon]}. \qquad \text{(A.2)}
\end{aligned}
$$

Explicit representations for the regular integrals can, e.g., be found in Ref. [15, 22]. The scalar integrals that involve mass-singular logarithms such as $\ln(m_f)$ or on-shell singularities such as $\ln(\hat{s} - M_\mathrm{W}^2 + \mathrm{i}\epsilon)$ are given by

$$
\begin{aligned}
B_0(m_1^2, 0, m_1) &= \Delta + 2 + \ln\Big(\frac{\mu^2}{m_1^2}\Big), \\
B_0(\hat{s}, 0, M_\mathrm{W}) &= \Delta + 2 + \ln\Big(\frac{\mu^2}{M_\mathrm{W}^2}\Big) + \Big(\frac{M_\mathrm{W}^2}{\hat{s}} - 1\Big)\ln\Big(1 - \frac{\hat{s}}{M_\mathrm{W}^2} - \mathrm{i}\epsilon\Big), \\
C_0(m_1^2, m_2^2, r, m_1, m_\gamma, m_2) &= \frac{1}{r}\Big\{\ln\Big(-\frac{r}{m_1 m_2} - \mathrm{i}\epsilon\Big)\ln\Big(-\frac{r}{m_\gamma^2} - \mathrm{i}\epsilon\Big) - \frac{1}{4}\ln\Big(-\frac{r}{m_1^2} - \mathrm{i}\epsilon\Big)^2 \\
&\qquad - \frac{1}{4}\ln\Big(-\frac{r}{m_2^2} - \mathrm{i}\epsilon\Big)^2 - \frac{\pi^2}{6}\Big\}, \\
C_0(m_1^2, 0, \hat{s}, 0, m_1, M_\mathrm{W}) &= \frac{1}{\hat{s}}\Big\{\ln\Big(\frac{\hat{s}}{m_1^2}\Big)\ln\Big(1 - \frac{\hat{s}}{M_\mathrm{W}^2} - \mathrm{i}\epsilon\Big) \\
&\qquad + \mathrm{Li}_2\Big(1 - \frac{\hat{s}}{M_\mathrm{W}^2} - \mathrm{i}\epsilon\Big) - \frac{\pi^2}{6}\Big\},
\end{aligned}
$$

$$C_0(m_1^2,0,M_{\rm W}^2,m_\gamma,m_1,M_{\rm W}) = \frac{1}{M_{\rm W}^2}\ln\Big(\frac{M_{\rm W}}{m_1}\Big)\ln\Big(\frac{m_\gamma^2}{m_1 M_{\rm W}}\Big), \tag{A.3}$$

where $m_\gamma^2 \ll m_{1,2}^2 \ll \hat{s}, |r|, M_{\rm W}^2$. The quantity $\Delta = 2/(4-D) - \gamma_{\rm E} + \ln(4\pi)$ is the standard UV divergence for $D \to 4$ space-time dimensions, and $\mu$ is the (arbitrary) reference mass scale of dimensional regularization.

## A.2 Box correction

In order to reduce the Dirac structure of the box diagrams to the structure

$$c_0 = [\bar{v}_d \gamma^\mu \omega_- u_u]\ [\bar{u}_{\nu_l} \gamma_\mu \omega_- v_l]\,, \tag{A.4}$$

which appears in the lowest-order matrix element $\mathcal{M}_0$, we used the identities

$$\begin{aligned}
[\bar{v}_d \not{k}_n \omega_- u_u]\ [\bar{u}_{\nu_l} \not{p}_u \omega_- v_l] &= -\hat{t} c_0/2, \\
[\bar{v}_d \gamma^\mu \gamma^\nu \gamma^\rho \omega_- u_u]\ [\bar{u}_{\nu_l} \gamma_\mu \gamma_\nu \gamma_\rho \omega_- v_l] &= 16 c_0, \\
[\bar{v}_d \gamma^\mu \gamma^\nu \not{k}_n \omega_- u_u]\ [\bar{u}_{\nu_l} \gamma_\mu \gamma_\nu \not{p}_u \omega_- v_l] &= -4\hat{t} c_0,
\end{aligned} \tag{A.5}$$

which are valid in four space-time dimensions.

The box correction factor $\delta_{\rm box}(\hat{s},\hat{t})$ introduced in (2.10) is explicitly given by

$$\begin{aligned}
\delta_{\rm box}(\hat{s},\hat{t}) = \frac{\alpha}{4\pi}(\hat{s}-M_{\rm W}^2)\Big\{ & \\
& (g_d^- g_l^- + g_{\nu_l}^- g_u^-)\Big[\, \frac{2}{\hat{u}}\Big(B_0(\hat{t},0,0) - B_0(\hat{s},M_{\rm W},M_{\rm Z})\Big) + 4C_0(0,0,\hat{s},M_{\rm W},0,M_{\rm Z}) \\
& \quad - \frac{M_{\rm W}^2 + M_{\rm Z}^2 + \hat{s} + 2\hat{t}}{\hat{u}^2}\Big(\hat{t}C_0(0,0,\hat{t},0,M_{\rm W},0) + \hat{t}C_0(0,0,\hat{t},0,M_{\rm Z},0) \\
& \qquad + 2\hat{s}C_0(0,0,\hat{s},M_{\rm W},0,M_{\rm Z})\Big) \\
& \quad - \frac{\hat{t}(M_{\rm W}^2 + M_{\rm Z}^2 + \hat{s} + 2\hat{t})^2 + 2(M_{\rm W}^2+\hat{t})(M_{\rm Z}^2+\hat{t})\hat{u}}{\hat{u}^2} D_0(0,0,0,0,\hat{t},\hat{s},0,M_{\rm W},0,M_{\rm Z}) \,\Big] \\
& - 2(g_d^- g_{\nu_l}^- + g_l^- g_u^-)\Big[\, 2C_0(0,0,\hat{s},M_{\rm W},0,M_{\rm Z}) - \hat{u} D_0(0,0,0,0,\hat{u},\hat{s},0,M_{\rm W},0,M_{\rm Z}) \,\Big] \\
& + Q_d Q_l \Big[\, \frac{2}{\hat{u}}\Big(B_0(\hat{t},0,0) - B_0(\hat{s},0,M_{\rm W})\Big) + 2C_0(m_d^2,0,\hat{s},0,m_d,M_{\rm W}) \\
& \quad + 2C_0(m_l^2,0,\hat{s},0,m_l,M_{\rm W}) - \frac{M_{\rm W}^2 + \hat{s} + 2\hat{t}}{\hat{u}^2}\Big(\hat{s}C_0(m_d^2,0,\hat{s},0,m_d,M_{\rm W}) \\
& \qquad + \hat{s}C_0(m_l^2,0,\hat{s},0,m_l,M_{\rm W}) + \hat{t}C_0(0,0,\hat{t},0,M_{\rm W},0) + \hat{t}C_0(m_d^2,m_l^2,\hat{t},m_d,m_\gamma,m_l)\Big) \\
& \quad - \hat{t}\Big(1 + \frac{(M_{\rm W}^2+\hat{t})^2}{\hat{u}^2}\Big) D_0(m_d^2,m_l^2,0,0,\hat{t},\hat{s},m_d,m_\gamma,m_l,M_{\rm W}) \,\Big] \\
& - 2Q_u Q_l \Big[\, C_0(m_l^2,0,\hat{s},0,m_l,M_{\rm W}) + C_0(m_u^2,0,\hat{s},0,m_u,M_{\rm W}) \\
& \quad - \hat{u} D_0(m_u^2,m_l^2,0,0,\hat{u},\hat{s},m_u,m_\gamma,m_l,M_{\rm W}) \,\Big] \,\Big\},
\end{aligned} \tag{A.6}$$

where $\hat{u} = -\hat{s} - \hat{t}$, and $g_f^-$ are the left-handed couplings of fermion $f$ to the Z boson,

$$g_f^- = \frac{I^3_{\mathrm{W},f}}{c_\mathrm{W} s_\mathrm{W}} - \frac{s_\mathrm{W}}{c_\mathrm{W}} Q_f. \tag{A.7}$$

The singular $D_0$ function is given by

$$\begin{aligned} D_0(m_1^2, m_2^2, 0, 0, r, \hat{s}, m_1, m_\gamma, m_2, M_\mathrm{W}) = \frac{1}{r(M_\mathrm{W}^2 - \hat{s})} \Big\{ \ln^2\Big(\frac{m_1}{M_\mathrm{W}}\Big) + \ln^2\Big(\frac{m_2}{M_\mathrm{W}}\Big) \\ + 2\ln\Big(-\frac{m_1 m_2}{r}\Big) \ln\Big(\frac{M_\mathrm{W}^2 - \hat{s}}{m_\gamma M_\mathrm{W}} - \mathrm{i}\epsilon\Big) + \frac{\pi^2}{3} + \mathrm{Li}_2\Big(1 + \frac{M_\mathrm{W}^2}{r}\Big) \Big\}, \end{aligned} \tag{A.8}$$

with $r = \hat{t}, \hat{u} < 0$.

# References


[1] A. Airapetian *et al.* (ATLAS Collaboration), "ATLAS Detector and Physics Performance: Technical Design Report, 2", CERN-LHCC-99-15, ATLAS-TDR-15.

[2] Z. Kunszt *et al.*, in *Physics at LEP2*, eds. G. Altarelli, T. Sjöstrand and F. Zwirner (CERN 96-01, Geneva, 1996), Vol. 1, p. 151 [hep-ph/9602352].

[3] H. Aihara *et al.*, "Future Electroweak Physics at the Fermilab Tevatron: Report of the TEV-2000 Study Group", FERMILAB-Pub-96/082.

[4] E. Accomando *et al.* [ECFA/DESY LC Physics Working Group Collaboration], Phys. Rept. **299** (1998) 1 [hep-ph/9705442];
J. A. Aguilar-Saavedra *et al.*, "TESLA Technical Design Report Part III: Physics at an $\mathrm{e}^+\mathrm{e}^-$ Linear Collider," hep-ph/0106315.

[5] A. D. Martin, R. G. Roberts, W. J. Stirling and R. S. Thorne, Eur. Phys. J. C **14** (2000) 133 [hep-ph/9907231].

[6] M. Dittmar, F. Pauss and D. Zürcher, Phys. Rev. D **56** (1997) 7284 [hep-ex/9705004].

[7] F. A. Berends and R. Kleiss, Z. Phys. C **27** (1985) 365.

[8] U. Baur, S. Keller and D. Wackeroth, Phys. Rev. D **59** (1999) 013002 [hep-ph/9807417].

[9] D. Wackeroth and W. Hollik, Phys. Rev. D **55** (1997) 6788 [hep-ph/9606398].

[10] R. Hamberg, W. L. van Neerven and T. Matsuura, Nucl. Phys. B **359** (1991) 343;
W. L. van Neerven and E. B. Zijlstra, Nucl. Phys. B **382** (1992) 11.

[11] U. Baur and T. Stelzer, Phys. Rev. D **61** (2000) 073007 [hep-ph/9910206].

[12] R. K. Ellis, D. A. Ross and S. Veseli, Nucl. Phys. B **503** (1997) 309 [hep-ph/9704239].

[13] S. Catani *et al.*, in *Proceedings of the workshop on standard model physics (and more) at the LHC*, eds. G. Altarelli and M. L. Mangano, (CERN 2000-04, Geneva, 2000), p. 1 [hep-ph/0005114].

[14] S. Haywood *et al.*, in *Proceedings of the workshop on standard model physics (and more) at the LHC*, eds. G. Altarelli and M. L. Mangano, (CERN 2000-04, Geneva, 2000), p. 117 [hep-ph/0003275].

[15] A. Denner, Fortsch. Phys. **41** (1993) 307.

[16] D. Y. Bardin, A. Leike, T. Riemann and M. Sachwitz, Phys. Lett. B **206** (1988) 539.

[17] W. Beenakker *et al.*, Nucl. Phys. B **500** (1997) 255 [hep-ph/9612260].

[18] H. Burkhardt and B. Pietrzyk, Phys. Lett. B **356** (1995) 398;
S. Eidelman and F. Jegerlehner, Z. Phys. C **67** (1995) 585 [hep-ph/9502298].

[19] J. Küblbeck, M. Böhm and A. Denner, Comput. Phys. Commun. **60** (1990) 165;
H. Eck and J. Küblbeck, *Guide to FeynArts 1.0*, University of Würzburg, 1992.

[20] G. Passarino and M. Veltman, Nucl. Phys. B **160** (1979) 151.

[21] R. Mertig, M. Böhm and A. Denner, Comput. Phys. Commun. **64** (1991) 345;
R. Mertig, *Guide to FeynCalc 1.0*, University of Würzburg, 1992.

[22] G. 't Hooft and M. Veltman, Nucl. Phys. B **153** (1979) 365;
W. Beenakker and A. Denner, Nucl. Phys. B **338** (1990) 349;
A. Denner, U. Nierste and R. Scharf, Nucl. Phys. B **367** (1991) 637.

[23] A. Denner, S. Dittmaier and G. Weiglein, Nucl. Phys. B **440** (1995) 95 [hep-ph/9410338].

[24] M. Passera and A. Sirlin, Phys. Rev. D **58** (1998) 113010 [hep-ph/9804309].

[25] A. Sirlin, Phys. Rev. D **22** (1980) 971;
W. J. Marciano and A. Sirlin, Phys. Rev. D **22** (1980) 2695 [Erratum-ibid. D **31** (1980) 213] and Nucl. Phys. B **189** (1981) 442.

[26] R. G. Stuart, Phys. Lett. B **262** (1991) 113;
A. Aeppli, F. Cuypers and G. J. van Oldenborgh, Phys. Lett. B **314** (1993) 413 [hep-ph/9303236];
H. Veltman, Z. Phys. C **62** (1994) 35.

[27] A. Denner, S. Dittmaier, M. Roth and D. Wackeroth, Nucl. Phys. B **587** (2000) 67 [hep-ph/0006307].

[28] S. Jadach, W. Placzek, M. Skrzypek, B. F. Ward and Z. Was, Phys. Lett. B **417** (1998) 326 [hep-ph/9705429];
W. Beenakker, F. A. Berends and A. P. Chapovsky, Nucl. Phys. B **548** (1999) 3 [hep-ph/9811481];

Y. Kurihara, M. Kuroda and D. Schildknecht, Nucl. Phys. B **565** (2000) 49 [hep-ph/9908486].

[29] M. W. Grünewald *et al.*, in *Reports of the Working Groups on Precision Calculations for LEP2 Physics*, eds. S. Jadach, G. Passarino and R. Pittau (CERN 2000-009, Geneva, 2000), p. 1 [hep-ph/0005309].

[30] K. Melnikov and O. Yakovlev, Nucl. Phys. B **471** (1996) 90 [hep-ph/9501358];
W. Beenakker, F. A. Berends and A. P. Chapovsky, Nucl. Phys. B **508** (1997) 17 [hep-ph/9707326].

[31] A. Denner, S. Dittmaier and M. Roth, Nucl. Phys. B **519** (1998) 39 [hep-ph/9710521].

[32] E. N. Argyres *et al.*, Phys. Lett. B **358** (1995) 339 [hep-ph/9507216].

[33] U. Baur and D. Zeppenfeld, Phys. Rev. Lett. **75** (1995) 1002 [hep-ph/9503344].

[34] S. Dittmaier, Phys. Rev. D **59** (1999) 016007 [hep-ph/9805445].

[35] F. A. Berends, R. Kleiss, P. De Causmaecker, R. Gastmans, W. Troost and T. T. Wu, Nucl. Phys. B **206** (1982) 61;
R. Kleiss, Z. Phys. C **33** (1987) 433.

[36] S. Dittmaier, Nucl. Phys. B **565** (2000) 69 [hep-ph/9904440].

[37] S. Catani and M. H. Seymour, Phys. Lett. B **378** (1996) 287 [hep-ph/9602277] and Nucl. Phys. B **485** (1997) 291 [Erratum-ibid. B **510** (1997) 291] [hep-ph/9605323].

[38] J. Kripfganz and H. Perlt, Z. Phys. C **41** (1988) 319;
H. Spiesberger, Phys. Rev. D **52** (1995) 4936 [hep-ph/9412286].

[39] C. Caso *et al.* [Particle Data Group Collaboration], Eur. Phys. J. C **3** (1998) 1.

[40] H. L. Lai *et al.*, Phys. Rev. D **55** (1997) 1280 [hep-ph/9606399].

[41] T. Kinoshita, J. Math. Phys. **3** (1962) 650;
T. D. Lee and M. Nauenberg, Phys. Rev. **133** (1964) B1549.

[42] V. A. Zykunov, hep-ph/0107059.